

AD-A013 641

EXPERIMENTAL INVESTIGATION OF CATAMARAN CROSS-STRUCTURE  
SLAMMING

Sheng-Lun Chuang, et al

Naval Ship Research and Development Center  
Bethesda, Maryland

September 1975

DISTRIBUTED BY:

**NTIS**

National Technical Information Service  
U. S. DEPARTMENT OF COMMERCE

238063

Report 4653

# NAVAL SHIP RESEARCH AND DEVELOPMENT CENTER

Bethesda, Md. 20084



AD A 0 1 3 6 4 1

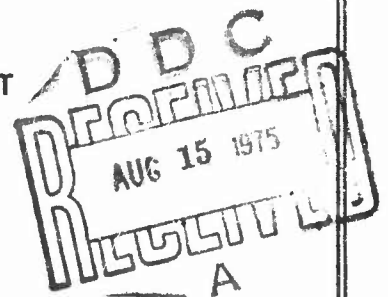
## EXPERIMENTAL INVESTIGATION OF CATAMARAN CROSS-STRUCTURE SLAMMING

by

Sheng-Lun Chuang,  
John T. Birmingham and Anthony J. Furio, Jr.

APPROVED FOR PUBLIC RELEASE: DISTRIBUTION UNLIMITED

STRUCTURES DEPARTMENT  
RESEARCH AND DEVELOPMENT REPORT



September 1975

Reproduced by  
NATIONAL TECHNICAL  
INFORMATION SERVICE  
U.S. Department of Commerce  
Springfield, VA 22151

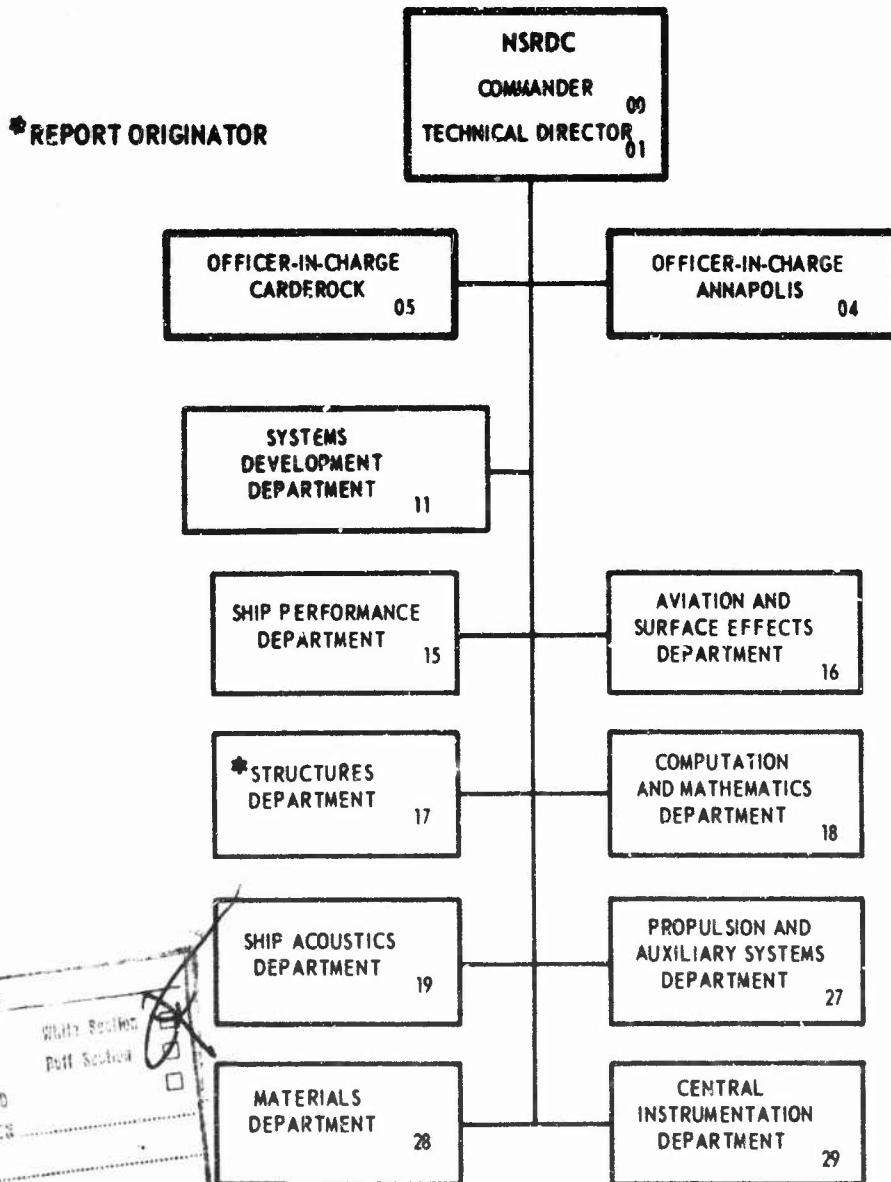
Report 4653

EXPERIMENTAL INVESTIGATION OF CATAMARAN CROSS-STRUCTURE SLAMMING

The Naval Ship Research and Development Center is a U. S. Navy center for laboratory effort directed at achieving improved sea and air vehicles. It was formed in March 1967 by merging the David Taylor Model Basin at Carderock, Maryland with the Marine Engineering Laboratory at Annapolis, Maryland.

Naval Ship Research and Development Center  
Bethesda, Md. 20084

### MAJOR NSRDC ORGANIZATIONAL COMPONENTS



ACCESSION for	
NTIS	White Section <input checked="" type="checkbox"/>
ORC	Puff Section <input type="checkbox"/>
UNANNOUNCED	
JUSTIFICATIONS	
BY _____	
DISTRIBUTION/AVAILABILITY CODES	
Dist.	AVAIL. ORG. OR SPECIAL
A	

*ii a*

**UNCLASSIFIED**

SECURITY CLASSIFICATION OF THIS PAGE (When Data Entered)

REPORT DOCUMENTATION PAGE		READ INSTRUCTIONS BEFORE COMPLETING FORM
1. REPORT NUMBER  4653	2. GOVT ACCESSION NO.	3. RECIPIENT'S CATALOG NUMBER
4. TITLE (and Subtitle)  EXPERIMENTAL INVESTIGATION OF CATAMARAN CROSS-STRUCTURE SLAMMING		5. TYPE OF REPORT & PERIOD COVERED
		6. PERFORMING ORG. REPORT NUMBER
7. AUTHOR(s)  Sheng-Lun Chuang, John T. Birmingham, and Anthony J. Furio, Jr.		8. CONTRACT OR GRANT NUMBER(s)
9. PERFORMING ORGANIZATION NAME AND ADDRESS  Naval Ship Research and Development Center Bethesda, Maryland 20084		10. PROGRAM ELEMENT, PROJECT, TASK AREA & WORK UNIT NUMBERS  Task Area SF 43 422 411/311 Work Unit 1-1730-341
11. CONTROLLING OFFICE NAME AND ADDRESS  Naval Sea Systems Command		12. REPORT DATE  September 1975
		13. NUMBER OF PAGES  55
14. MONITORING AGENCY NAME & ADDRESS (if different from Controlling Office)		15. SECURITY CLASS. (of this report)  <b>UNCLASSIFIED</b>
		15a. DECLASSIFICATION/DOWNGRADING SCHEDULE
16. DISTRIBUTION STATEMENT (of this Report)  APPROVED FOR PUBLIC RELEASE: DISTRIBUTION UNLIMITED		
17. DISTRIBUTION STATEMENT (of the abstract entered in Block 20, if different from Report)		
18. SUPPLEMENTARY NOTES  NAVSEA exploratory development effort on structural testing of catamarans		
19. KEY WORDS (Continue on reverse side if necessary and identify by block number)  Elasticity Effect on Slamming Load      Catamaran Model Test Slamming Load Prediction                  Full Scale Catamaran Slamming Load Slamming of Catamaran Cross-Structure    Load-Area Relation for Slamming Load Structural Response to Slamming		
20. ABSTRACT (Continue on reverse side if necessary and identify by block number)  A model of a conventional catamaran was tested in regular head waves at the Naval Ship Research and Development Center to investigate the cross-structure slamming phenomenon. The severity of slamming was found to be determined principally by the relative motions resulting from the ship's pitch and heave and the relations of these motions with the impacting wave surface. The impact pressure prediction method that was developed on the basis of  (Continued on reverse side)		

DD FORM 1 JAN 73 1473

EDITION OF 1 NOV 68 IS OBSOLETE \*  
S/N 0102-014-6601 |

**UNCLASSIFIED**

SECURITY CLASSIFICATION OF THIS PAGE (When Data Entered)

**UNCLASSIFIED**

**SECURITY CLASSIFICATION OF THIS PAGE(When Data Entered)**

(Block 20 continued)

these findings gave results that agreed reasonably well with the data from model tests and full-scale sea trials on USNS HAYES (T-AGOR-16). Spatial averages of impact pressures obtained from the model and full-scale data provide pressure-area relations for use in determining load criteria for cross-structure bottom plate, panel, and grillage design. The effect of deformability of impact surfaces was also investigated and the results used to provide guidance in the development of load criteria for the structural design of the cross structure in the slamming area.

**UNCLASSIFIED**

**SECURITY CLASSIFICATION OF THIS PAGE(When Data Entered)**

## TABLE OF CONTENTS

	Page
ABSTRACT . . . . .	1
ADMINISTRATIVE INFORMATION . . . . .	1
INTRODUCTION . . . . .	1
PREDICTION OF SLAMMING PRESSURE . . . . .	2
METHOD I (REGULAR OR IRREGULAR WAVES) . . . . .	6
METHOD II (REGULAR WAVES ONLY) . . . . .	8
EXPERIMENTAL METHOD . . . . .	11
DESCRIPTION OF MODELS . . . . .	11
TEST PROCEDURE . . . . .	11
INSTRUMENTATION SYSTEM . . . . .	13
RESULTS AND DISCUSSION . . . . .	13
EXPERIMENTAL AND PREDICTED PEAK SLAMMING PRESSURES . . . . .	13
SLAMMING PRESSURE DISTRIBUTION . . . . .	20
EFFECT OF DEFORMABILITY OF IMPACT SURFACE . . . . .	28
EFFECTS OF CROSS-STRUCTURE CLEARANCE, SHIP SPEED, WAVE CELERITY, AND WAVE HEIGHT . . . . .	30
ADDITIONAL EXPERIMENTAL FINDINGS . . . . .	32
CONSIDERATIONS FOR THE PRACTICAL STRUCTURAL DESIGN OF CROSS STRUCTURE IN THE SLAMMING AREA . . . . .	33
DETERMINATION OF PEAK IMPACT PRESSURE . . . . .	34
STRUCTURAL RESPONSE . . . . .	34
SUMMARY AND CONCLUSIONS . . . . .	35
ACKNOWLEDGMENTS . . . . .	37
APPENDIX A – ANALYSES OF HAYES SEA TRIAL CROSS- STRUCTURE SLAMMING DATA . . . . .	39
APPENDIX B – METHODS OF DATA COLLECTION AND REDUCTION . . . . .	43
REFERENCES . . . . .	48

## LIST OF FIGURES

	Page
1 - Comparison of Peak Impact Pressures Determined by Various Methods . . . . .	4
2 - Velocity Diagram for Method I—Regular or Irregular Waves . . . . .	7
3 - Velocity Diagram for Method II—Regular Waves Only . . . . .	10
4 - ASR Model in Towing Position . . . . .	12
5 - Gage Locations . . . . .	14
6 - Comparisons of Predicted and Measured Peak Slamming Pressures . . . . .	19
7 - Area Used to Take Average Impact Pressures at Forward Section of Cross Structure . . . . .	27
8 - Relative Wave Impact Pressure on Bottom of Cross Structure versus Ship Station . . . . .	29
9 - Maximum Pressure versus Wave Impact Surface Area . . . . .	29
10 - Impact Pressure Records . . . . .	31
A.1 - Predicted and Measured Peak Pressure Factor k versus Impact Angle for HAYES as Built . . . . .	41
B.1 - Sample Record for Elastic Model . . . . .	45
B.2 - Determination of Pitch Velocity . . . . .	46
B.3 - Determination of Heave Velocity . . . . .	46
B.4 - Determination of Pitch Angle . . . . .	47
B.5 - Determination of Wave Slope . . . . .	47

## LIST OF TABLES

1 - Computer Program for Predicting Slamming Pressure by Method I . . . . .	9
2 - Computer Results by Method I . . . . .	16
3 - Measured Pressure Distribution at Forward Section of Cross-Structure Model . . . . .	21
A.1 - Summary of HAYES Slamming Data and Computer Results . . . . .	40

## NOTATION

Symbol	Definition	Dimensions
AGOR	Auxiliary oceanographic research catamaran class	
ASR	Auxiliary submarine rescue ship class	
$g$	Gravitational acceleration	feet per second <sup>2</sup>
$h$	Maximum wave amplitude measured from calm water surface	feet
$k$	A constant	
$k_1$	Wave number = $2\pi/L_w$	per foot
$L_w$	Wave length	feet
LCG	Longitudinal center of gravity	feet
$l$	Distance between LCG and impact point	feet
$n$	Number of readings	
$p_{ave}$	Average pressure	pounds per square inch
$p_i$	Impact pressure	pounds per square inch
$p_{max}$	Peak pressure	pounds per square inch
$p_p$	Planing pressure	pounds per square inch
$p_t$	Total pressure normal to impact surface	pounds per square inch
$t$	Time in general	seconds
$T_w$	Wave period	seconds
VCG	Vertical center of gravity	feet
$V_{hea}$	Heave velocity	feet per second
$V_h$	Ship speed	feet per second
$V_k$	Ship speed	knots
$V_n$	Velocity normal to wave surface	feet per second
$V_{n0}$	Normal velocity of water particle at wave surface	feet per second
$V_{ns}$	Velocity normal to impact surface	feet per second

Symbol	Definition	Dimensions
$V_0$	Water orbiting velocity	feet per second
$V_p$	Linear pitch velocity = $\dot{\theta}_p \xi$	feet per second
$V_t$	Tangential velocity to wave surface	feet per second
$V_{t0}$	Tangential velocity of water particle at wave surface	feet per second
$V_v$	Relative vertical velocity	feet per second
$V_w$	Wave celerity	feet per second
$V_{wav}$	Vertical velocity of wave surface measured at impact point of moving impact body	feet per second
$y$	Wave distance measured from a point where $\theta_w = \theta_{max}$	feet or % $L_w$
$\beta$	Deadrise angle	degrees or radians
$\theta_r$	Rolling angle	degrees or radians
$\theta_w$	Wave slope	degrees or radians
$\theta_{max}$	Maximum wave slope	degrees or radians
$\theta_0$	Orbiting angle	degrees or radians
$\theta_F$	Pitch angle	degrees or radians
$\dot{\theta}_p$	Angular pitch velocity	degrees per second or radians per second
$\xi$	Impact angle = $\theta_p + \theta_w$	degrees or radians
$\rho$	Mass density of fluid	slug (i.e., lb-sec <sup>2</sup> /ft <sup>4</sup> )

## NOTATION USED IN COMPUTER PROGRAM

Symbol	Definition	Dimensions
AK	k in Equations (1) and (2)	
C	Calculated k by $(PNR-PPC)/(1.94 VN^2)$	
PIC	Calculated $p_i$	pounds per square inch
PNC	Calculated $p_t$	pounds per square inch
PNR	Recorded $p_t$	pounds per square inch
PPC	Calculated $p_p$	pounds per square inch
RD	$\theta_r$	degrees
T	$\theta_p$	radians
TD	$\theta_p$	degrees
VHEA	$V_{hea}$	feet per second
VN	$V_n$	feet per second
VNS	$V_{ns}$	feet per second
VP	$V_p$	feet per second
VT	$V_t$	feet per second
VV	$V_v$	feet per second
VWAV	$V_{wav}$	feet per second
WS	$\theta_w$	radians
WSD	$\theta_w$	degrees
X	$\xi$	degrees
XI	$\xi$	radians

## ABSTRACT

A model of a conventional catamaran was tested in regular head waves at the Naval Ship Research and Development Center to investigate the cross-structure slamming phenomenon. The severity of slamming was found to be determined principally by the relative motions resulting from the ship's pitch and heave and the relations of these motions with the impacting wave surface. The impact pressure prediction method that was developed on the basis of these findings gave results that agreed reasonably well with the data from model tests and full-scale sea trials on USNS HAYES (T-AGOR-16). Spatial averages of impact pressures obtained from the model and full-scale data provide pressure-area relations for use in determining load criteria for cross-structure bottom plate, panel, and grillage design. The effect of deformability of impact surfaces was also investigated and the results used to provide guidance in the development of load criteria for the structural design of the cross structure in the slamming area.

## ADMINISTRATIVE INFORMATION

The experimental investigation was carried out at the Naval Ship Research and Development Center (NSRDC) and was sponsored by the Naval Ship Systems Command (now Naval Sea Systems Command-NAVSEA) with exploratory development funds Task Area SF 43 422 311. Data analyses and reporting were funded by NAVSEA with exploratory development funds under Task Area SF 43 422 411. Publication of this report was funded under Work Unit 1-1730-341.

## INTRODUCTION

Twin-hull ships, including conventional catamarans and small waterplane area twin hulls (SWATH), have attracted much attention in recent years because of their special suitability for certain types of service. Their principal advantages over conventional monohulls include larger deck area and volume for a specific displacement and, in the case of SWATH, improved seakeeping.

Despite the fact that twin-hull ships create new design problems in many areas, their structural design (particularly that of the conventional catamaran) has relied, until recently, on existing technology for monohull ships. One of the major problems is that validated wave impact (slamming) load design criteria have not been established. Slamming, described as an unsteady hydrodynamic impact phenomenon, is often poorly predicted by available

technology even for monohull surface ships. Catamarans experience slamming loads most frequently on the under side of the forward cross structure.

In view of this deficiency in slamming load criteria, NSRDC conducted several fundamental theoretical and experimental studies to clarify the basic concept of slamming.<sup>1</sup> Since most models used for the experiments had wedge-shaped impact bodies, application of these experimental results to the structural design of the slamming areas of ship hulls requires more experimental verification, particularly as applied to the cross structure of the multihull ship. The objectives of the present series of investigations are:

1. To establish experimentally the levels of realistic slamming loads (or pressures) and load distribution acting on a rigid as well as a deformable impact surface of the cross structure.
2. To correlate experimental results with a method for predicting slamming pressure.
3. To provide guidance for determining load criteria for the structural design of the cross structure in the slamming area.

During sea trials of USNS HAYES (T-AGOR-16), the first oceangoing catamaran of the U.S. Navy, the ship experienced cross-structure slamming. Some of these slamming data were analyzed to determine slamming pressures by means of the prediction method given in this report. These results are summarized and compared in Appendix A.

## PREDICTION OF SLAMMING PRESSURE

A method for predicting the three-dimensional peak slamming pressure in waves was partially developed some time ago.<sup>2,3</sup> Later this method was further developed, and verified by the results of slamming tests of three-dimensional models in both calm water and waves.<sup>4</sup> Since the impact of the cross structure on a wave surface involves pitch and heave as well as wave motion, equations used for predicting peak slamming pressures must be modified slightly to suit the present impact conditions. However, the approaches used to obtain these equations are identical to those employed previously.

Chuang<sup>4</sup> demonstrated that even though the moving body had a velocity in a direction other than normal to the impact surface, the pressure is affected only by the velocity

---

<sup>1</sup>Chuang, S.L., "Investigation of Impact of Rigid and Elastic Bodies with Water," NSRDC Report 3248 (Feb 1970). A complete list of references is given on page 48.

<sup>2</sup>Chuang, S.L., "Impact Pressure Distributions on Wedge-Shaped Hull Bottoms of High-Speed Craft," NSRDC Report 2953 (Aug 1969).

<sup>3</sup>Chuang, S.L., "Design Criteria for Hydrofoil Hull Bottom Plating," NSRDC Report 3509 (Jan 1971).

<sup>4</sup>Chuang, S.L., "Slamming Tests of Three-Dimensional Models in Calm Water and Waves," NSRDC Report 4095 (Sep 1973).

component normal to the impact surface. Furthermore, the pressure which acts normal to the impact surface in the slamming area can be separated into two components:

1. The impact pressure  $p_i$  due to the normal velocity component of the impact body normal to the wave surface.
2. The planing pressure  $p_p$  due to the normal velocity component of the impact body tangential to the wave surface.<sup>4</sup>

To estimate the peak impact pressure  $\text{Max } p_i$ , the pressure-velocity relation may be expressed in the general form (see Figure 1)

$$\text{Max } p_i = k \rho V_n^2 \quad (1)$$

where  $k$  = an arbitrary constant

$\rho$  = mass density of fluid in pounds-seconds<sup>2</sup> per foot<sup>4</sup>

$V_n$  = normal velocity component to the wave surface in feet per second.

The impact pressure  $p_i$  is in pounds per square inch.

The values of  $k$  for wedges and cones can be determined from the Wagner wedge impact theory,<sup>5</sup> the Chuang cone impact theory,<sup>6</sup> and NSRDC drop tests of wedges and cones.<sup>7</sup> When the impact angles  $\xi$  are small, the  $k$  values determined by these different methods deviate considerably, especially the comparisons between theoretical and experimental values (see Figure 1), and it is reasonable to believe that the experimental values are more realistic. Moreover, since the three-dimensional hull form is within the limits of wedge-shaped and cone-shaped bodies, the  $k$  values for the impact of the cross structure may be approximated by the dotted line (labeled "3-D prediction") shown in Figure 1. This dotted line can be expressed by equations obtained by curve fitting methods.<sup>8</sup> These equations are:

---

<sup>5</sup>Wagner, V.H., "Über Stosz- und Gleitvorgänge an der Oberfläche von Flüssigkeiten," *Zeitschrift für Angewandte Mathematik und Mechanik*, Vol. 12, No. 4, pp. 193-215 (Aug 1932).

<sup>6</sup>Chuang, S.L., "Theoretical Investigations on Slamming of Cone-Shaped Bodies," *Journal of Ship Research*, Vol. 13, No. 4 (Dec 1969).

<sup>7</sup>Chuang, S.L. and D.T. Milne, "Drop Tests of Cones to Investigate the Three-Dimensional Effects of Slamming," NSRDC Report 3543 (Apr 1971).

<sup>8</sup>Carnahan, B. et al., "Applied Numerical Methods," Chapter 1, John Wiley & Sons, Inc., New York (1969).

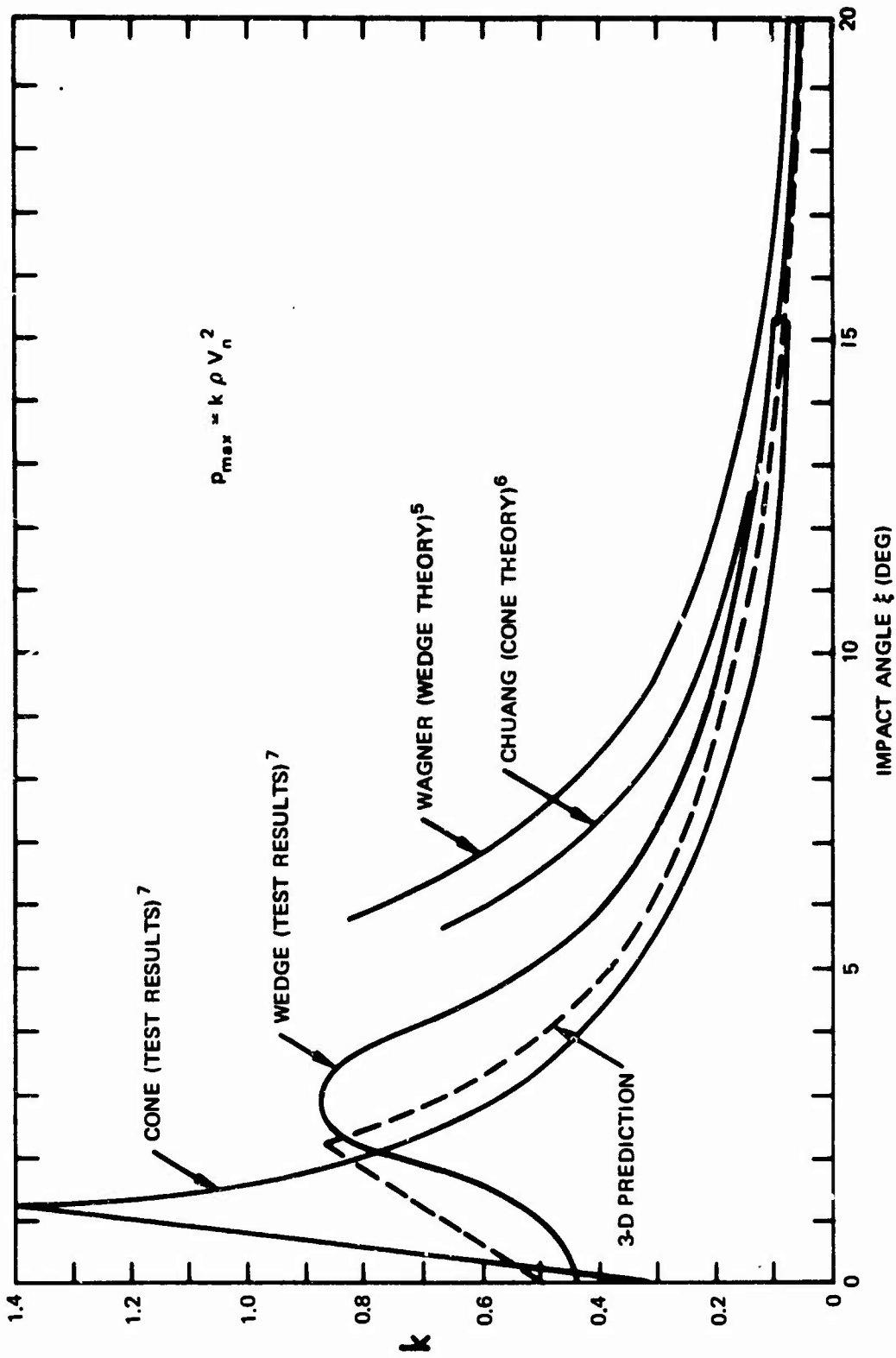


Figure 1 - Comparison of Peak Impact Pressures Determined by Various Methods

(Here  $P_{max}$  in pounds per square inch,  $\rho$  in slug, and  $V_n$  in feet per second; tests were performed in calm water.)

1. For  $0 \leq \xi < 2.2$  deg:

$$k = 0.045833 \xi^2 + 0.149167 \xi + 0.32$$

2. For  $2.2 \leq \xi < 11$  deg:

$$k = 2.1820894 - 0.9451815 \xi + 0.2037541 \xi^2 \\ - 0.0233896 \xi^3 + 0.0013578 \xi^4 - 0.00003132 \xi^5$$

3. For  $11 \leq \xi < 20$  deg:

$$k = 4.748742 - 1.3450284 \xi + 0.1576516 \xi^2 \\ - 0.0092976 \xi^3 + 0.0002735 \xi^4 - 0.00000319864 \xi^5$$

4. For  $20 \text{ deg} \leq \xi$ , (Modified Wagner formula):

$$k = (1 + 2.4674/\tan^2 \xi) 0.76856471/288$$

(2)

Since the models had flat bottom surfaces, the impact angle is simply the sum of the ship pitch angle  $\theta_p$  at the time of impact and the wave slope  $\theta_w$  at the point of impact on the wave surface, i.e.,

$$\xi = \theta_p + \theta_w \quad (3)$$

This equation applies to the cross structure with a horizontal flat bottom. If it is sloped fore and aft due to ship trim, then the trim angle is added to the equation. Other configurations of the impact bottom surface will require the use of equations given earlier by Chiang.<sup>4</sup>

The planing pressure acting normal to the impact surface is<sup>3</sup>

$$\text{Max } p_p = \frac{1}{2} \rho V_t^2 (1/144) \quad (4)$$

The total pressure due to velocity components of the impact surface both normal and tangent to the wave surface is therefore

$$p_t = p_i + p_p \quad (5)$$

usually  $p_p$  is much smaller than  $p_i$  and may be neglected without serious error.

In Equations (4) and (5),  $V_t$  is the tangential velocity in feet per second, and both the planing pressure  $p_p$  and the total pressure  $p_t$  are in pounds per square inch. The value of the mass density of fluid  $\rho$  is simply the unit weight of fluid divided by the gravitational acceleration  $g$ .

The values of  $V_n$  in Equation (1) and  $V_t$  in Equation (4) may be determined by one of two methods. The first, Method I, considers the vertical movement of the wave surface and the second, Method II, considers the orbiting velocity of water particles at the wave surface.

## METHOD I (REGULAR OR IRREGULAR WAVES)

Consider that the catamaran moves with pitch and heave motions in the waves. At the time of impact, the catamaran has a pitch angle of  $\theta_p$ . Let the coordinate system move with the catamaran at a fixed point where motions are recorded (Figure 2), and also let

$V_{\text{hea}}$  = heave velocity measured at LCG of moving catamaran

$V_{\text{wav}}$  = vertical velocity of wave surface measured at the impact point of moving catamaran (i.e., when the catamaran moves with horizontal velocity  $V_h$  and the wave moves with wave celerity  $V_w$ .)

$V_p$  = linear pitch velocity at the impact point

The relative vertical velocity  $V_v$  is then

$$V_v = V_{\text{hea}} - V_{\text{wav}}$$

The velocity component  $V_{ns}$  normal to the impact surface is then the sum of the  $V_v$  component normal to the impact surface and  $V_p$  the linear pitch velocity which is normal to the impact surface, i.e.,

$$\begin{aligned} V_{ns} &= V_v \cos \theta_p + V_p \\ &= (V_{\text{hea}} - V_{\text{wav}}) \cos \theta_p + V_p \end{aligned}$$

Since the angular pitch velocity  $\dot{\theta}_p$  is measured, the linear pitch velocity  $V_p$  at the impact point can be obtained by the equation

$$V_p = \dot{\theta}_p \ell \quad (6)$$

where  $\ell$  is the distance between the longitudinal center of gravity (LCG) and the particular impact point of concern.

Since the pulse of the impact pressure lasts only a few milliseconds, the event of impact occurs only at and very near the wave surface of the sea. Therefore, it is reasonable to assume that the impact velocity is equal to the relative velocity between the impact surface of the moving body and the wave surface. Based on this hypothesis, the normal and the tangential velocities of the impact surface to the wave surface are

$$V_n' = V_{ns} \cos (\theta_p - \theta_w)$$

$$V_t = V_{ns} \sin (\theta_p - \theta_w)$$

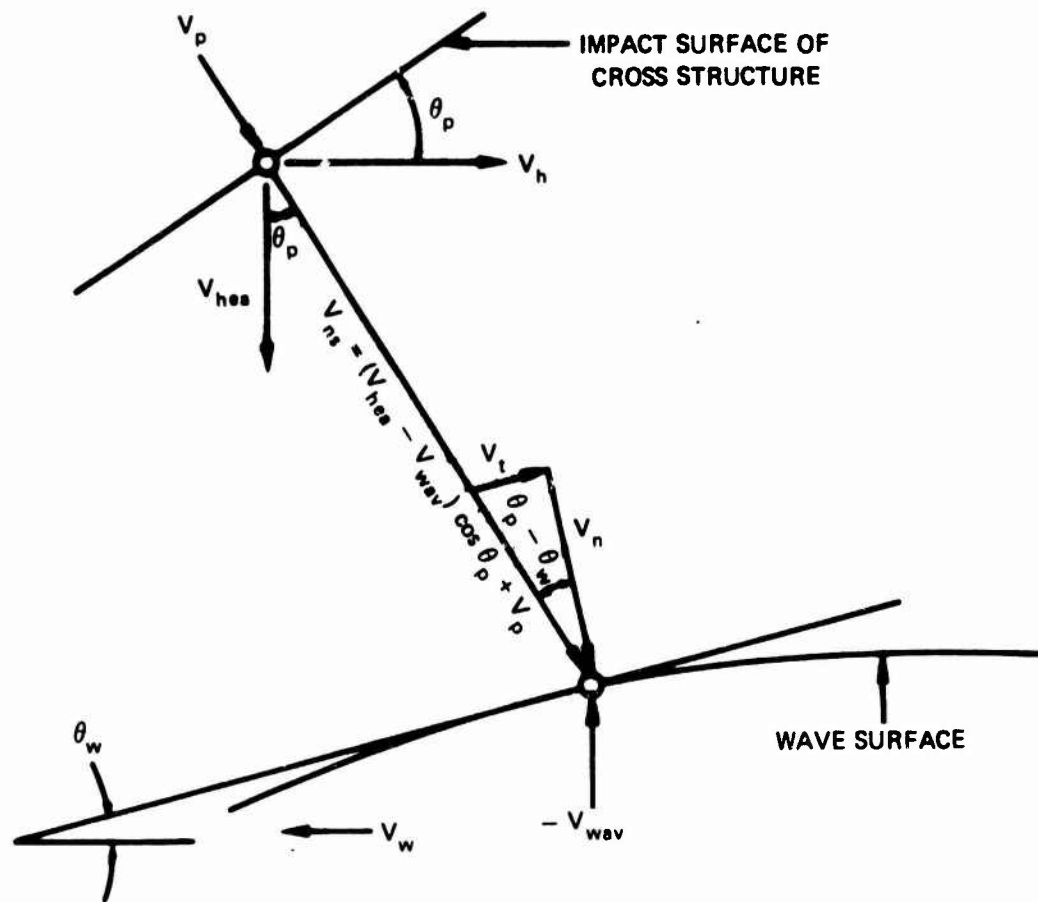


Figure 2 – Velocity Diagram for Method I--Regular or Irregular Waves

Since the  $V_n'$  used for estimating the impact pressure by Equation (1) has been referred to as  $V_v$  for Equation (2) when the wave slope  $\theta_w$  is zero, it is necessary to divide  $V_n'$  by  $\cos^2 \theta_p$  so that Equations (1) and (2) can be used for the present prediction. Then the combination of the above equations and  $V_n = V_n' / \cos^2 \theta_p$  becomes

$$\left. \begin{aligned} V_{ns} &= (V_{hea} - V_{wav}) \cos \theta_p + V_p \\ V_n &= V_{ns} \cos(\theta_p - \theta_w) / \cos^2 \theta_p \\ V_t &= V_{ns} \sin(\theta_p - \theta_w) \end{aligned} \right\} (7)$$

The vertical movement of the wave surface  $V_{wav}$  is produced by the horizontal movements of the impact body and the wave celerity. Although neither the ship speed nor the wave celerity is involved in the equation, these two terms are actually included in  $V_{wav}$ . The computer program for this method (Method I) is given in Table 1.

#### METHOD II (REGULAR WAVES ONLY)

If the orbital motion of water particles is considered and if the wave is regular, the wave surface has the following properties (Figure 3):

$$\left. \begin{aligned} \text{Wave number:} & \quad k_1 = 2\pi/L_w \\ \text{Orbiting velocity:} & \quad V_0 = k_1 h V_w \\ \text{Wave slope:} & \quad \theta_w = k_1 h \cos k_1 (y - V_w t) \\ \text{Maximum wave slope:} & \quad \theta_{max} = k_1 h \\ \text{Normal velocity:} & \quad V_{n_0} = V_0 \cos(\theta_0 + \theta_w) \\ \text{Tangential velocity:} & \quad V_{t_0} = V_0 \sin(\theta_0 + \theta_w) \\ \text{Orbiting angle:} & \quad \theta_0 = k_1 (y - V_w t) \end{aligned} \right\} (8)$$

Consider that the ship has horizontal velocity  $V_h$ , heave velocity  $V_{hea}$ , and pitch velocity  $V_p$ . Then, similar to the previous method of derivation,

TABLE 1 - COMPUTER PROGRAM FOR PREDICTING  
SLAMMING PRESSURE BY METHOD I

```

100 PROGRAM CAT(INPUT,OUTPUT)
110C PREDICTION OF SLAMMING PRESSURE OF CATAMARAN
120C RUN NO
125C CASE NO
130 TD=PITCH ANGLE IN DEG
140 PNR=RECORDED IMPACT PRESSURE IN PSI
150 WSD=WAVE SLOPE IN DEG
160 X=TD-WSD
170 T=.0174533*TD
180 WS=.0174533*WSD
190 XI=.0174533*X
191 VHEA=HEAVE VELOCITY IN FPS
192 VWAV=VERTICAL VELOCITY OF WAVE SURFACE IN FPS
193 VV=VHEA-VWAV
194 VP=VERTICAL VELOCITY DUE TO PITCH ,FPS
200 VNS=VV*COS(T)+VP
210 VN=(VNS*COS(XI))/(COS(T)**2)
220 VT=VNS*SIN(XI)
230 PPC=0.006736*(VT*VT)
240 X=ABS(X)
250 IF(2.2-X)20,20,10
260 10 AK=.37*X/2.2+.5
270 GO TO 45
280 20 IF(11.-X)30,30,25
290 25 AK=2.1820894-.9451815*X+.2037541*X**2-.0233896*X**3
300 AK=AK+.0013578*X**4-.00003132*X**5
310 GO TO 45
320 30 IF(20.-X)40,40,35
330 35 AK=4.748742-1.3450284*X+.1576516*X**2-.0092976*X**3
340 AK=AK+.0002735*X**4-.00000319864*X**5
350 GO TO 45
360 40 AK=.76856471*(1.+2.4674/(TAN(XI)**2))/288.
370 45 PIC=1.94*AK*VN**2
380 PNC=PPC+PIC
381 C=(PNR-PPC)/(1.94*VN**2)
390 PRINT 80,VN,VT,X,C
400 80 FORMAT(2X,11H VN(FPS) = ,F7.3,11H VT(FPS) = ,F7.3,
405 + 11H X(DEG) = ,F7.3,6H C = ,F5.3)
410 PRINT 100,AK,PNC,PNR
420 100 FORMAT(8X,5H K = ,F7.5,11H PNC(PSI)= ,F7.3,
430 + 11H PNR(PSI)= ,F7.3)
440 STOP
450 END

```

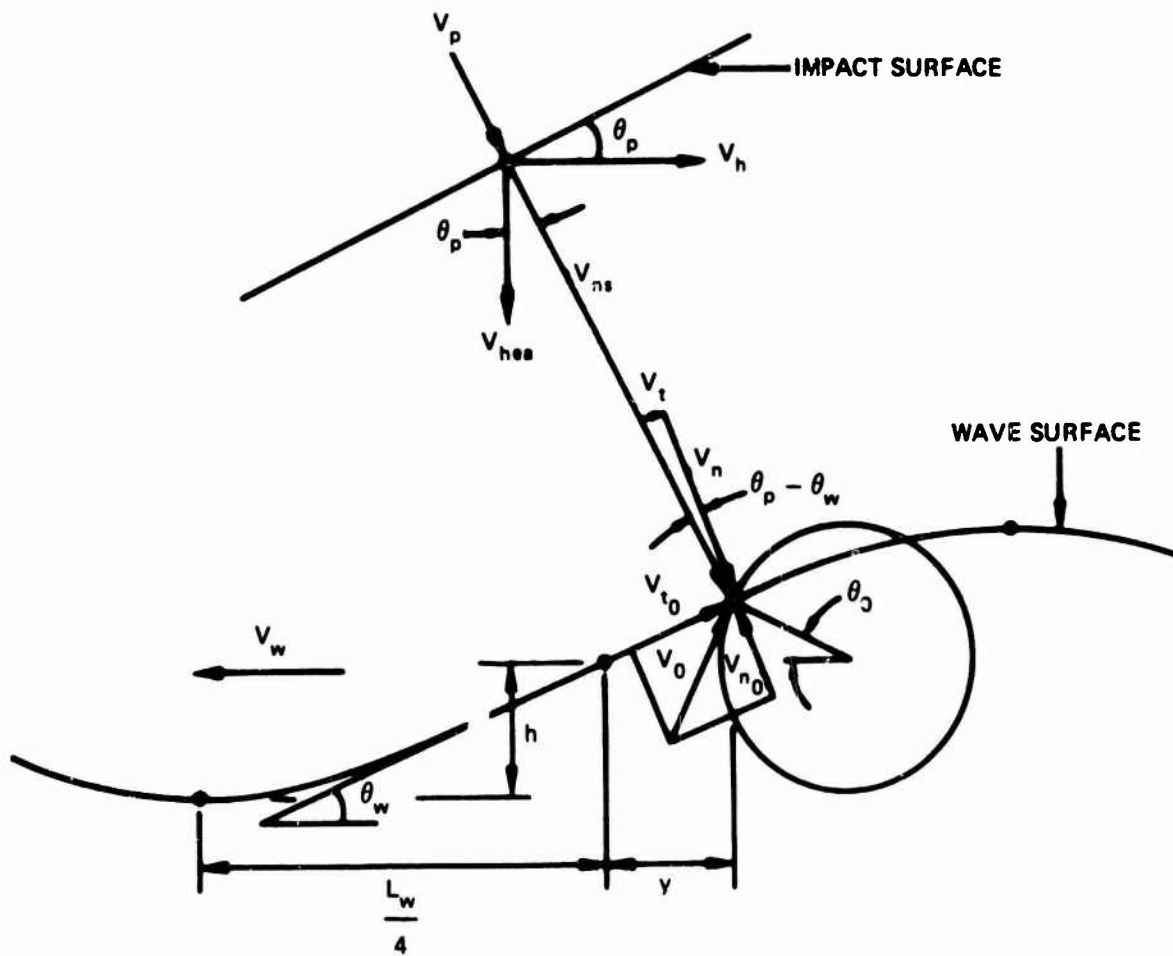


Figure 3 – Velocity Diagram for Method II—Regular Waves Only

$$\begin{aligned}
 V_{ns} &= V_{hea} \cos \theta_p + V_h \sin \theta_p + V_p \\
 V_n &= V_{ns} \cos(\theta_p - \theta_w) / \cos^2 \theta_p + V_{n_0} \\
 V_t &= V_{ns} \sin(\theta_p - \theta_w) - V_{t_0}
 \end{aligned}
 \quad \left. \vphantom{\begin{aligned} V_{ns} \\ V_n \\ V_t \end{aligned}} \right\} (9)$$

## EXPERIMENTAL METHOD

### DESCRIPTION OF MODELS

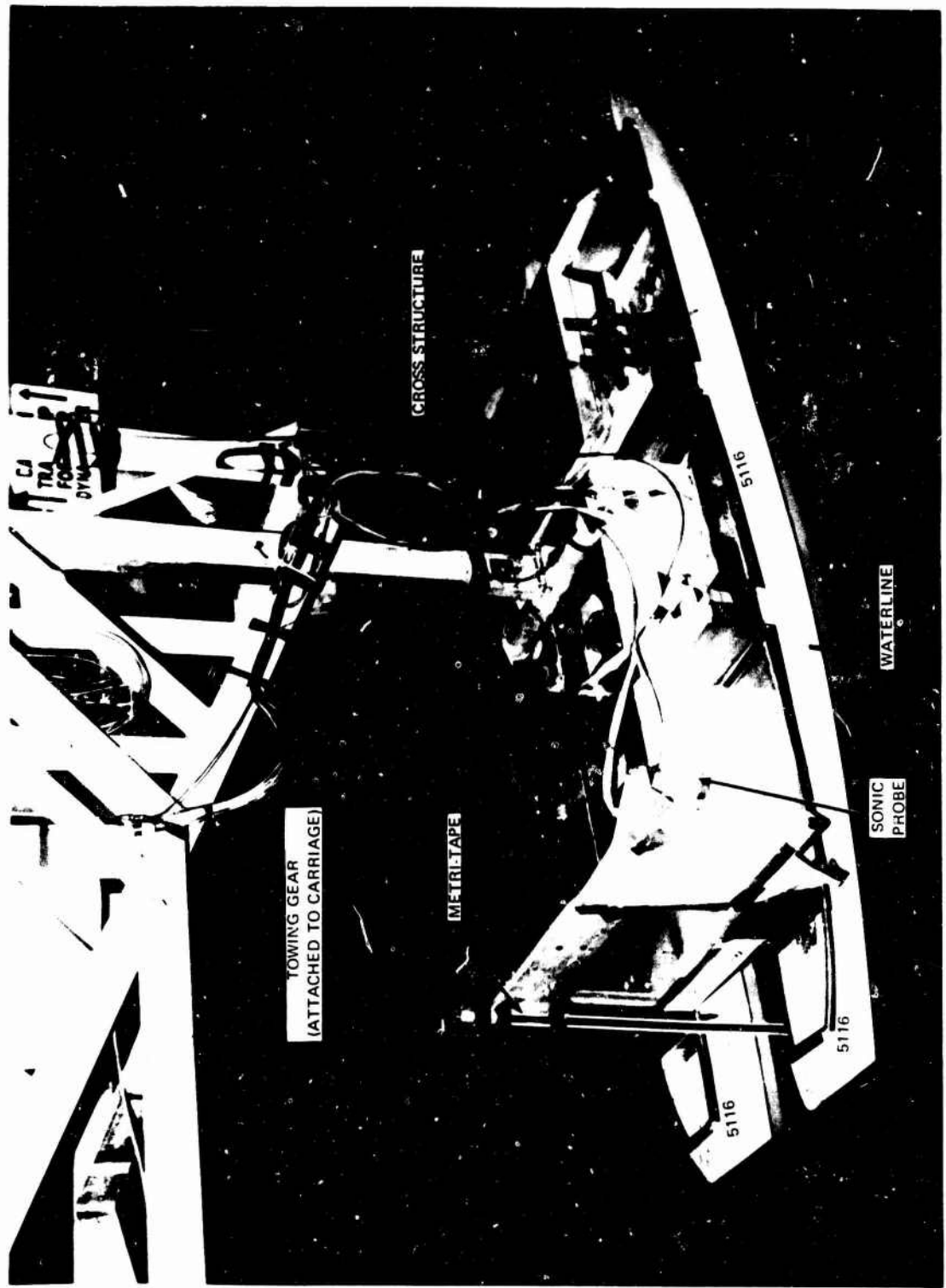
An existing ASR catamaran model was utilized for the present series. The model and the test arrangement are shown in Figure 4. This model was designated NSRDC Model 5116 and represented the final design of an auxiliary submarine rescue ship (ASR-21). Each hull of the model was 10.91 ft long and 1.22 ft wide with a draft of 0.89 ft and a scale ratio of 21.28. The total width of the model was 4.04 ft with a 19-in. wide cross structure between the two hulls; its total weight was 800 lb.

The cross-structure model sections were made of aluminum. Two sets of cross-structure models were tested, one with 1/4-in. bottom plate panels for rigid body impact and the other with 1/32-in. plate for deformable body impact. Each cross-structure model consisted of three separated boxes which could be raised or lowered either together or independently to achieve different clearances of the cross structure above the water. The length of the box was 32 in., and the total length of the cross structure was 8 ft. The box was 19 in. wide and was located between two hulls. Three heights of cross structure were tested, i.e., 4 1/4, 7 1/4, and 10 1/4 in. above the water surface.

### TEST PROCEDURE

The model was tested and towed at its LCG in *regular wave and head seas only* with a speed-length ratio of up to 1.0 (or model speed up to 3.3 knots). The tank-generated waves ranged in length from less than 10 ft to a little over 30 ft and in height up to about 2 ft crest-to-trough.

Details of the test assembly can be viewed in Figure 4. The model was attached to the towing gear and the gear was attached to the towing carriage. The towing gear was guided and free to move in the vertical direction only, and the model was free to rotate in pitch



Reproduced from  
best available copy.

Figure 4 - ASR Model in Towing Position

only at the intersection of its LCG and VCG. The carriage traveled at a constant speed during each test run. Pressures, accelerations, deflections, pitch, heave, wave height, and relative displacement between the wave surface and the moving bow of the model were recorded. Locations of these transducers are shown in Figure 5. Methods of data collection and reduction are given in Appendix B.

## **INSTRUMENTATION SYSTEM**

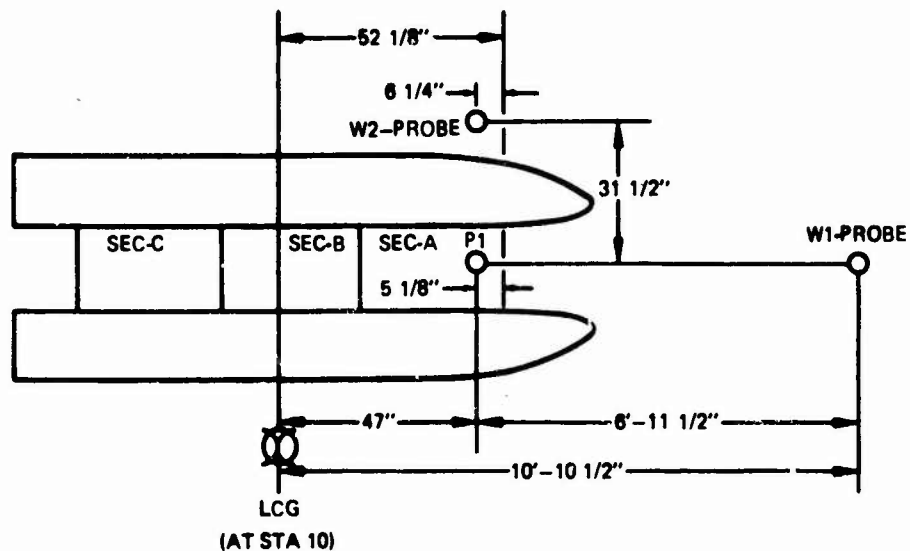
A detailed description of the instrumentation has already been given; see Appendix A in Chuang and Milne.<sup>7</sup> Briefly, it consisted of quartz-crystal pressure transducers, charge amplifiers, d-c amplifiers, and a tape recorder. The entire recording system had the ability to pick up and record any high-frequency acoustic pressure caused by the impact of the moving body on the water surface. In addition, two sonic probes were installed, one at the towing carriage in front of the model for measuring the wave profile during the course of impact of the model on the waves and one attached to the model for measuring the relative displacement between the wave surface and the model at the bow. These locations are indicated in Figure 5.

## **RESULTS AND DISCUSSION**

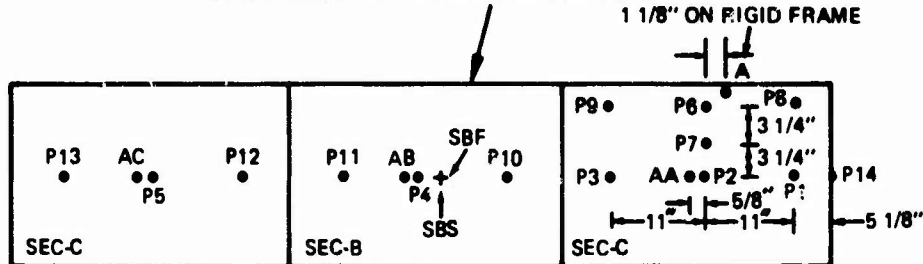
The test results presented and discussed in this section are divided into four areas: (1) the peak impact pressure at a selected point where the highest impact pressure is likely to occur; (2) the average impact pressure at a selected area where impact is likely to occur; (3) the effect of the deformation of the impact surface on the impact pressure; and (4) other effects on the impact pressure, such as cross-structure clearance, ship speed, wave celerity, etc.

### **EXPERIMENTAL AND PREDICTED PEAK SLAMMING PRESSURE**

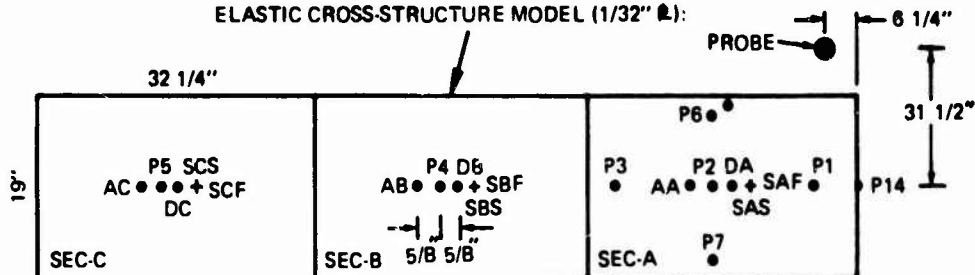
Examination of experimental records indicated that the highest peak pressures usually occurred at the P1 pressure gage which was placed at the foremost centerline location of the cross structure (see Figure 5 for location). The finding was not unexpected since the cross-structure model had a flat bottom and the highest peak impact pressure should have occurred at its centerline location.<sup>1</sup> Therefore, the P1 pressures were in reasonable agreement with the values obtained from predictions.



(AT STA 10)  
RIGID CROSS-STRUCTURE MODEL (1/4"  $\square$ ):



ELASTIC CROSS-STRUCTURE MODEL (1/32"  $\square$ ):



- P1-P13 = PRESSURE GAGES (LOCATED UNDERSIDE OF CROSS-STRUCTURE)
- P14 = PRESSURE GAGE (LOCATED FORE BHD)
- A, AA, AB, AC = ACCELEROMETERS
- DA, DB, DC = DEFLECTION GAGES
- SAF, SBF, SCF = STRAIN GAGES
- SAS, SBS, SCS = STRAIN GAGES
- W2-PROBE = WAVE PROBE TO MEASURE RELATIVE WAVE HEIGHT
- W1-PROBE = WAVE PROBE TO MEASURE WAVE HEIGHT

PITCH AND HEAVE MEASURED AT CENTER OF GRAVITY OF MODEL

Figure 5 - Gage Locations

The records showed a great many test runs that were not characteristic of slamming in regular waves. For example, the impacting wave surfaces may have been somewhat distorted or irregular. The peaks of the impact pressures generated by these imperfect slammings were damped and much below the predicted values, e.g., Run 387, Cases II and III of Table 2. For that reason, only those slamming events with generally typical or characteristic pressure pulse profiles were analyzed and compared with the predictions.

Method I was used for the predictions because most wave records showed the irregularity noted above and thus it was difficult to determine wave orbiting velocity with reasonable accuracy as required by Method II. Method I uses the vertical velocity of the wave surface at a given point, and this can be determined from the wave record. Other velocities were obtained from Equation (7). The calculated and recorded values of the peak impact pressures are summarized in Table 2. Considering the difficulty in defining such wave properties as velocities, wave surface, impact angles, etc. that affect the prediction results, the agreement is considered very good.

Perhaps the greatest uncertainty during the test involved measurement of the wave profile. Because the wavemeter, a sonic probe, was located several feet from the model (see Figure 5 for location), some discrepancy undoubtedly existed between the measured wave profile and the wave profile at the point of impact.

Also shown in Table 2 are the  $k$  values calculated from the equation

$$\text{Recorded max } P_t - \text{Calculated } P_p = k \rho V_n^2$$

Figure 6 compares these  $k$  values with the prediction line for the three-dimensional slamming indicated in Figure 1. Again, the agreement is very good.

The angles of the cross-structure bottom impact  $\xi$ , shown in Figure 6, are not the deadrise angles of the model  $\beta$ . Since the bottoms of the cross-structure models are flat, the values of deadrise angles are always zero. But the angle of impact  $\xi$  varies up to 20 deg or more. The angle of impact  $\xi$  for the present case is the sum of the pitch angle and the wave slope, as given by Equation (3).

The second method of prediction (Method II, which considers the orbiting velocity of the water particles of the wave) was used for a limited number of cases. The comparisons between predictions and test results were also considered reasonably good. However, since further studies are needed, the presentation is omitted at the present time.

TABLE 2 - COMPUTER RESULTS BY METHOD I

TABLE 2a - RIGID CROSS-STRUCTURE MODEL AT LOW POSITION (4 1/4 IN. CLEARANCE)

Run	T <sub>w</sub> sec	V <sub>k</sub> knots	Case	θ <sub>D</sub> deg	θ <sub>w</sub> deg	ξ deg	V <sub>hpa</sub> fps	V <sub>wav</sub> fps	V <sub>p</sub> fps	k Eq (1),(2)	k Computer	Rec'd P <sub>i</sub>	Calc. P <sub>i</sub>
9	1.4	0.66	I	-9.45	0	9.45	1.73	0	1.97	0.175	0.126	3.41	4.72
			II	4.45	-1.53	2.92	0.82	0.22	0.81	0.669	1.074	3.07	1.91
12	1.4	1.98		-4.45	-1.22	3.23	0.86	0.15	1.60	0.604	0.604	8.3	8.29
21	1.4	1.98		-3.34	4.03	7.37	1.02	-0.74	0	0.245	0.438	2.6	1.45
23	1.71	0.66	I	-3.89	3.44	7.33	0.81	-0.59	1.29	0.247	0.347	4.82	3.43
			II	-0.11	3.23	9.34	1.04	-0.56	1.29	0.178	0.232	3.73	2.86
24	1.71	1.32		-6.11	2.90	9.01	1.25	-0.56	1.21	0.167	0.181	2.83	3.29
25	1.71	1.85		-6.67	3.31	9.98	1.21	0.67	1.36	0.163	0.140	2.83	3.28
31	1.71	1.32		-7.64	0	7.64	1.29	0	1.64	0.234	0.179	3.02	3.94
36	1.71	0.66		-8.55	8.1	14.65	1.16	-1.397	1.15	0.086	0.091	2.31	2.18
37	1.71	1.32	I	-8.18	0	8.18	1.81	0	1.19	0.214	0.139	2.44	3.77
			II	-8.18	0	8.18	2.18	0	1.64	0.214	0.218	6.23	8.12
			III	-7.08	3.55	10.63	1.7	-0.88	1.04	0.150	0.110	2.57	3.49
			IV	-10.90	0	10.90	1.77	0	1.64	0.145	0.134	3.09	3.33
39	1.71	1.98	I	-4.91	9.3	14.21	0.27	1.96	1.19	0.090	0.122	2.63	1.94
			II	-8.54	-5.01	1.53	1.98	1.06	0.71	0.757	0.661	3.47	3.98
			III	-8.72	3.4	12.12	2.34	-0.72	1.41	0.117	0.119	4.56	4.48

Note: For Runs 31, 36, 37, and 39, the midsection was raised to the high position, and the forward and aft end sections remained at the low position.

TABLE 2b - RIGID CROSS-STRUCTURE MODEL AT MIDPOSITION (7 1/4 IN. CLEARANCE)

Run	T <sub>w</sub> sec	V <sub>k</sub> knots	Case	θ <sub>D</sub> deg	θ <sub>w</sub> deg	ξ deg	V <sub>hpa</sub> fps	V <sub>wav</sub> fps	V <sub>p</sub> fps	k Eq (1),(2)	k Computer	Rec'd P <sub>i</sub>	Calc. P <sub>i</sub>
41	1.71	0.66	I	-8.61	3.86	11.99	1.59	-0.58	1.37	0.120	0.126	3.02	2.87
			II	-9.16	6.51	15.67	1.45	-1.12	1.44	0.077	0.099	2.96	2.31
69	2.4	2.64	I	-8.89	3.56	12.45	2.87	-1.04	-0.76	0.112	0.112	2.1	2.09
			II**	-8.39	5.58	14.47	3.04	-1.63	-0.43	0.087	0.067	2.23**	2.93
72*	1.71	1.32	I	-7.78	-0.77	7.01	2.15	0.15	1.12	0.260	0.135	>4.52*	8.69
			II	-8.89	4.46	13.35	2.26	-0.85	0.76	0.099	0.131	3.71	2.81
88	1.71	0.66		-8.33	7.23	15.56	1.34	-1.25	1.44	0.078	0.166	5.0	2.35
89	1.71	0.66		-15.6	-4.6	11.00	2.26	0.79	1.9	0.143	0.126	3.02	3.43
91	1.71	1.65		-8.33	0.56	8.89	2.41	-0.11	0.87	0.191	0.158	3.54	4.27
92	1.71	1.98	I	-10.00	0	10.00	2.34	0	1.52	0.162	0.138	4.05	4.75
			II	-5.68	8.95	14.61	0.98	-1.89	0.69	0.086	0.146	3.41	2.01
96	1.71	0		-13.80	-5.42	8.38	1.85	0.83	2.43	0.207	0.136	3.41	5.18
115	2.0	0.66		-10.55	0	10.55	2.51	0	1.25	0.151	0.173	4.81	4.20
122	2.0	1.32		-7.22	0	7.22	1.75	0	0.68	0.251	0.279	3.21	2.89
124	2.0	1.98	I	-8.9	1.43	10.33	2.37	-0.34	0.68	0.55	0.168	3.73	3.45
			II	-8.9	0	8.9	1.97	0	0.95	0.191	0.192	3.21	3.18

\* P1 = 4.27, P8 = 4.52, therefore recorded p<sub>i</sub> should be greater than 4.52 psi.  
 \*\* Record damped

TABLE 2c - RIGID CROSS-STRUCTURE MODEL AT HIGH POSITION (10 1/4 IN. CLEARANCE)

Run	T <sub>w</sub> sec	V knots	Case	θ <sub>p</sub> deg	θ <sub>w</sub> deg	ξ deg	V <sub>hea</sub> fps	V <sub>wav</sub> fps	V <sub>p</sub> fps	k Eq. (1),(2)	k Computer	Rec'd P <sub>i</sub>	Calc. P <sub>i</sub>
131	1.71	1.32		- 9.23	8.77	18.00	1.91	-1.30	1.85	0.074	0.105	5.01	3.54
133	1.71	1.98		- 8.08	8.41	18.49	1.83	-1.78	-0.24	0.070	0.069	1.42	1.46
136	1.71	1.32		- 8.08	5.33	13.41	1.83	-1.04	0.79	0.098	0.094	2.12	2.22
137	1.71	1.65		- 6.35	6.97	13.32	2.0	-1.41	0.39	0.099	0.048	1.3	2.68
140	1.71	1.32		-10.4	3.09	13.49	1.83	-0.59	0.37	0.097	0.095	1.41	1.45
142	1.71	1.98		- 6.92	3.51	10.43	2.08	-0.74	0	0.153	0.135	2.05	2.32
145	1.4	1.65		- 8.08	5.75	13.83	1.23	-1.00	0.32	0.094	0.113	1.38	1.14
154	2.0	2.64		- 8.92	2.31	9.23	1.67	-0.59	-0.42	0.181	0.168	1.09	1.17

TABLE 2d - ELASTIC CROSS-STRUCTURE MODEL AT MIDPOSITION

Run	T <sub>w</sub> sec	V <sub>k</sub> knots	Case	θ <sub>p</sub> deg	θ <sub>w</sub> deg	ξ deg	V <sub>hea</sub> fps	V <sub>wav</sub> fps	V <sub>p</sub> fps	k Eq. (1),(2)	k Computer	Rec'd P <sub>i</sub>	Calc. P <sub>i</sub>
192	1.4	1.85		- 3.92	0.871	4.79	0.954	-0.151	0.308	0.365	0.664	2.57	1.52
206	1.4	1.98		- 8.259	3.203	11.46	1.892	-0.588	1.36	0.131	0.103	2.833	3.33
211	1.71	1.85		-11.001	2.822	13.922	2.83	-0.59	1.03	0.093	0.088	3.34	3.52
212	1.71	1.98	I	-13.211	3.713	16.92	3.231	-0.784	0.95	0.067	0.064	3.019	3.16
			II	- 8.257	7.431	15.69	2.365	-1.569	0.64	0.077	0.088	3.404	2.97
218	2.0	1.65		-11.01	5.174	16.18	3.231	-1.176	1.33	0.073	0.112	6.937	4.50
251	1.71	1.32		- 6.792	7.924	14.72	1.495	-1.519	1.13	0.085	0.085	2.698	2.71
253	1.71	1.98		- 6.792	7.196	13.99	2.039	-1.519	1.01	0.092	0.086	3.340	3.58
254	1.71	2.64		-11.321	6.423	17.74	1.728	-1.481	1.05	0.062	0.080	2.698	2.09
256*	2.0	1.32		-13.019	-0.848	12.17	3.612	0.185	2.11	0.116	0.092	5.625*	7.11
257**	2.0	1.65		-10.189	6.028	16.72	4.097	-1.37	0.78	0.073	0.069	5.03**	5.27
259	2.0	2.64		-12.453	1.301	12.75	3.748	-0.333	0.35	0.095	0.102	3.854	3.58

\* P1 = 5.074 P2 = 5.625 (used)

\*\* P1 = 4.111 P2 = 5.03 (used)

TABLE 2e - ELASTIC CROSS-STRUCTURE MODEL AT LOW POSITION

Run	T <sub>w</sub> sec	V <sub>k</sub> knots	Case	θ <sub>p</sub> deg	θ <sub>w</sub> deg	ξ deg	V <sub>hee</sub> fps	V <sub>wav</sub> fps	V <sub>p</sub> fps	k Eq. (1),(2)	k Computer	Rec'd p <sub>i</sub>	Calc. p <sub>i</sub>
307	1.71	1.32		- 9.5	0	9.50	1.86	0	1.90	0.174	0.108	2.7	4.34
317	1.4	1.32	I	- 7.22	-0.29	6.93	1.31	0.04	1.71	0.264	0.177	3.08	4.60
			II	- 9.45	-0.89	8.56	1.87	0.13	2.51	0.202	0.170	6.1	7.21
324	1.71	1.32	I	- 9.06	-0.95	8.10	2.1	0.18	0.93	0.217	0.232	3.7	3.47
			II	-10.2	-1.9	8.30	1.71	0.38	2.40	0.210	0.146	4.1	5.91
326	1.71	1.86		- 7.92	0	7.92	2.06	0	1.08	0.24	0.156	3.5	4.31
327	1.71	1.98		- 6.22	-1.5	4.32	1.41	0.4	1.39	0.442	0.408	4.62	5.00
330	2.0	0	I	-12.44	1.86	14.09	2.0	-0.3	2.62	0.091	0.073	3.47	4.33
			II	-11.86	-0.62	11.24	1.8	0.11	2.05	0.137	0.144	3.6	3.42
332	2.0	1.32		-10.75	-1.0	9.75	2.82	0.22	1.51	0.168	0.138	4.62	5.61
347	1.71	1.32		- 9.62	0	9.62	2.55	0	1.86	0.171	0.081	3.1	6.53
352*	2.0	0.66		-15.3	0	15.30	2.61	0	2.08	0.080	0.081	3.8*	3.53
359	2.0	1.98		-10.2	0	10.20	3.14	0	1.24	0.158	0.125	4.7	5.93

\* P1 - 3.6 (used), P2 - 3.04, P6 - 4.21 psi

TABLE 2f - ELASTIC CROSS-STRUCTURE MODEL AT HIGH POSITION

Run	T <sub>w</sub> sec	V <sub>k</sub> knots	Case	θ <sub>p</sub> deg	θ <sub>w</sub> deg	ξ deg	V <sub>hee</sub> fps	V <sub>wav</sub> fps	V <sub>p</sub> fps	k Eq. (1),(2)	k Computer	Rec'd p <sub>i</sub>	Calc. p <sub>i</sub>
387	2.0	1.85	I	-13.05	-0.32	12.73	2.87	0.08	0.62	0.107	0.132	3.02	2.45
			II*	-11.9	-1.44	10.48	2.73	0.33	0.81	0.153	0.065	1.32*	3.12
			III*	-11.9	-2.07	9.83	2.80	0.48	1.24	0.166	0.065	1.64*	4.20
388	2.0	1.98		- 9.5	1.23	11.03	3.08	-0.29	1.16	0.142	0.124	4.95	5.67
391	1.55	1.65		-11.88	5.45	17.33	2.12	-1.02	0.97	0.065	0.085	2.70	2.05
394	1.85	0		-13.6	3.96	17.56	1.96	-0.66	1.20	0.063	0.062	1.74	1.76
396	1.85	1.32	I	-13.0	-1.87	11.13	3.20	0.378	1.31	0.140	0.085	2.89	4.77
			II	-11.0	3.99	14.99	3.14	-0.813	1.37	0.083	0.075	4.05	4.45
400	1.4	1.32		-11.9	8.92	18.82	2.96	-1.13	0.93	0.057	0.083	3.85	2.26
407	1.71	1.98	I	-11.3	5.02	16.32	2.70	-1.06	-0.16	0.072	0.189	4.56	1.73
			II	-11.3	3.70	15.00	2.18	-0.94	-0.23	0.083	0.155	2.44	1.30
409	2.0	0.66		-18.4	-3.81	12.59	3.54	0.755	0.70	0.109	0.184	4.56	2.71
411	2.0	1.65	I	-12.5	-2.82	9.68	3.46	0.64	0.085	0.169	0.130	2.18	2.83
			II	-14.7	6.96	21.66	3.83	-1.59	0.93	0.044	0.045	3.34	3.28
413	2.0	2.64		-13.02	4.42	17.44	4.31	-1.13	-0.74	0.064	0.060	2.44	2.62

\* Recorded pressure pulse damped

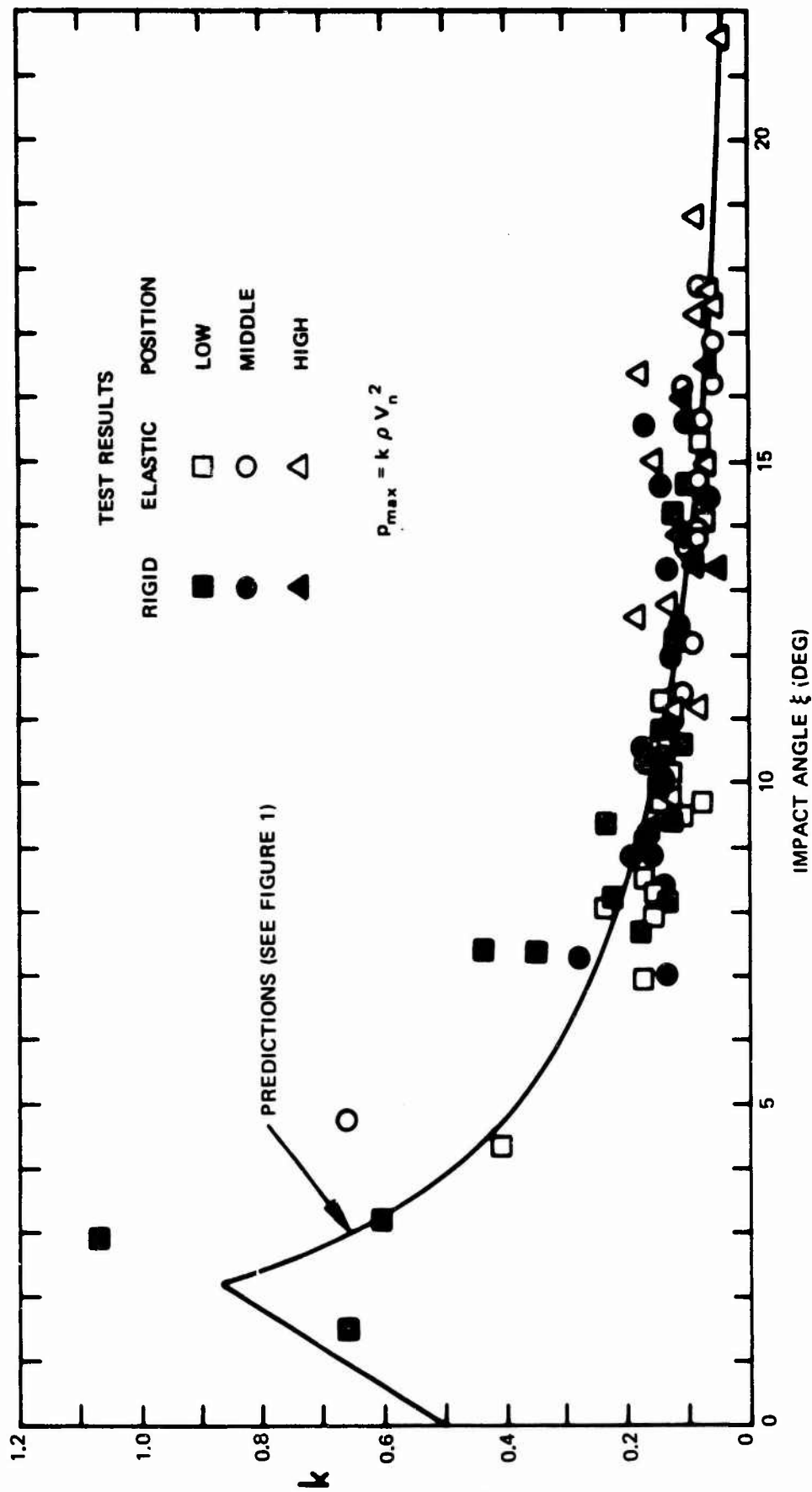


Figure 6 - Comparisons of Predicted and Measured Peak Slamming Pressures  
 ( $P_{max}$  is in pounds per square inch,  $\rho$  in slugs, and  $V_n$  in feet per second)

## SLAMMING PRESSURE DISTRIBUTION

The experimental records showed that there was little or no slamming at the midsection of the cross structure, some slamming at its aft section, and more serious slamming at the forward section. Thus slamming pressure distribution was checked for the entire bottom of the forward section.

The locations of pressure gages on the forward section for both the rigid and the deformable-body models are indicated in Figure 5. Since all records showed that all the pressure pulses were very irregular in shape, the same weight was applied to average those pressure readings at any prescribed time  $t$ . For the rigid-body model, five different averages were taken for the pressure readings of the forward section area; these averages were tabulated and are given in Table 3. The five averages\* are

$$p_{ave} I = [p_1 + p_2 + p_3 + p_8 + p_9 + (p_6 + p_7)/2]/6$$

$$p_{ave} II = [p_1 + p_2 + p_3 + (p_6 + p_7)/2]/4$$

$$p_{ave} III = [p_1 + p_8]/2$$

$$p_{ave} IV = [p_1 + p_8 + p_2 + (p_6 + p_7)/2]/4$$

$$p_{ave} V = [p_2 + (p_6 + p_7)/2]/2$$

The areas used to take the average impact pressures at the forward section of the cross structure are indicated by the shaded areas in Figure 7. For the elastic model, only  $p_{ave} II$  was tabulated; it is also given in Table 3.

The experimental records showed that when the impact angle with the wave surface was not zero during slamming, the peak pressures at individual points did not occur at the same time. Therefore, it is obvious that the localized peak pressure is higher than the average pressure over a larger area. Their differences generally depend on the sizes of impact angles. If the angles are small, their differences are small; if the angles are large, their differences are large. The data in Table 3 and Figure 7 also indicate that the average pressure is usually less over the larger area than over the smaller area. For example, as indicated in Table 3,

---

\* Averaging readings were taken at the same instant.

**TABLE 3 – MEASURED PRESSURE DISTRIBUTION OF FORWARD SECTION BOTTOM OF CROSS-STRUCTURE MODEL**

(Values shown are maximum pressures in pounds per square inch. The highest pressure in each event is indicated by a single asterisk. Values too small to read are indicated by a double asterisk.)

**TABLE 3a – RIGID MODEL AT LOW POSITION (4 1/4 IN. CLEARANCE)**

Run	Event	Case Shown in Table 2	P1	P2	P3	P6	P7	P8	P <sub>ave I</sub>	P <sub>ave II</sub>	P <sub>ave III</sub>	P <sub>ave IV</sub>	P <sub>ave V</sub>
9	1		1.3*	0.3	0.05	0.1	0.15	0.45	0.15	0.2			
	2		0.25	0.4	—**	0.3	0.4	2.50*	0.42	0.25			
	3		0.5	1.5	—	2.0*	0.6	0.4	0.50	0.70			
	4		1.05	1.4*	1.0	0.9	0.55	0.85	0.30	0.45			
	5		0.45	0.6*	0.35		0.4	0.3	0.30	0.45			
	6		0.7	2.65*	0.1	0.5	0.3	—	0.35	0.55			
	7	I	3.4*	1.9	0.5	1.2	1.35	1.2	0.55	0.95			
	8		1.2	1.5*	0.4	1.3	0.9	1.2	0.45	0.65			
	9	II	3.1	4.1*	0.1	0.3	1.1	1.5	0.95	1.25			
12	1		2.1*	1.4	0.1	0.2	0.9	4.1	0.60	0.75			
	2	I	6.3*	1.05	0.15	0.4	0.55	0.55	1.05	1.65			
	3		2.45	1.7	—	0.4	0.7	4.7*	0.80	0.60			
	4		1.3*	0.85	—	0.25	0.45	0.7	0.3	0.45			
	5		2.1*	0.4	—	0.5	0.2	1.2	0.35	0.45			
	6		2.7	0.9	—	0.6	0.5	4.0*	0.67	0.55			
	7		2.4*	1.4	—	0.2	0.6	1.3	0.5	0.55			
	8		1.75*	1.7	—	0.3	0.5	0.75	0.35	0.45			
	9		2.0*	0.65	—	0.15	0.25	1.15	0.35	0.50			
23	1		1.5	5.0*	—	1.0	1.35	1.5	0.75	1.1			
	2		1.1*	0.8	0.5	0.3	0.5	0.6	0.25	0.45			
	3		1.4	1.75	2.3	2.7*	1.3	1.1	0.6	0.9			
	4		1.4*	1.4*	0.4	0.55	0.85	0.7	0.55	0.8			
	5	II	3.8	3.0	0.1	1.75	1.6	4.2*	0.8	1.2			
24	1		2.4*	1.8	0.4	0.8	1.3	1.4	0.45	0.8			
	2	I	2.9*	0.45	0.3	0.25	0.1	0.35	0.45	0.75			
	3		1.6*	0.65	0.25	0.65	0.3	0.90	0.25	0.35			
	4		0.7*	0.25	—	0.35	0.15	0.5	0.15	0.2			
	5		0.7*	0.4	0.15	0.2	0.15	0.5	0.15	0.15			
	6		0.45	0.65*	0.2	0.2	0.2	0.5	0.10	0.15			

TABLE 3a (Continued)

Run	Event	Case Shown in Table 2	P1	P2	P3	P6	P7	P8	P <sub>ave</sub> I	P <sub>ave</sub> II	P <sub>ave</sub> III	P <sub>ave</sub> IV	P <sub>ave</sub> V
31	1		1.0*	0	0	0	0	0.35	0.15	0.25			
	2		2.2*	0.35	—**	0.3	0.4	0.7	0.45	0.65			
	3	I	3.1*	2.9	0.5	1.45	1.4	0.9	0.60	0.95			
	4		0.5*	0.15	—	0.1	0.1	0.5*	0.10	0.15			
	5		1.1	1.25*	0.1	0.5	0.8	0.75	0.30	0.40			
	6		1.65*	0.9	—	0.25	0.45	0.5	0.25	0.40			
	7		1.15	1.45*	0.3	0.2	0.6	0.85	0.30	0.45			
37	1		0.45	1.4*	0.25	0.7	0.8	0.2	0.25	0.45	0.35	0.45	0.75
	2		0.25	0.4*	0.15	0.05	0.25	0.1	0.15	0.25	0.15	0.2	0.3
	3	I	2.5*	2.05	1.15	1.0	1.1	2.35	0.55	0.75	1.6	0.8	1.35
	4		0.5	1.2*	0.5	0.5	0.5	0.85	0.25	0.30	0.3	0.3	0.65
	5		1.2	1.4*	0.05	0.25	0.7	0.75	0.4	0.60	0.85	0.65	0.8
	6	III	2.6	0.95	—	0.7	0.75	4.5*	0.65	0.55	2.7	1.25	0.5
	7	IV	3.1*	1.45	0.2	0.6	0.6	1.85	0.7	0.80	2.4	1.15	0.9
39	1		2.2*	1.5	0.3	0.5	0.7	2.0	0.4	0.45	1.8	0.9	0.7
	2		0.7	0.95	—	—	0.1	1.35*	0.15	0.2	0.6	0.3	0.5
	3	I	2.7*	0.55	—	0.2	0.2	0.6	0.5	0.7	1.8	0.8	0.35
	4		2.6*	1.6	—	0.9	1.6	1.2	0.65	0.85	1.3	1.0	1.1
	5		1.4	1.75	0.3	1.0	1.0	2.1*	0.6	0.70	1.4	0.8	1.25
40	1		1.95*	1.05	—	0.3	0.95	0.55	0.5	0.80	1.0	0.8	0.75
	2		3.1	4.0*	0.7	2.0	3.5	1.2	1.3	1.75	1.9	1.95	2.2
	3		0.55	1.1*	—	0.5	1.05	0.1	0.25	0.35	0.3	0.35	0.7
	4		0.7	0.6	0.1	0.2	0.25	1.9*	0.20	0.20	0.9	0.4	0.3
	5		2.0	2.4*	—	0.8	1.4	0.9	0.5	0.70	1.05	0.9	1.1

\*Highest maximum pressures within the event. \*\* Values too small to read.

NOTES: P<sub>ave</sub> I = 1/6 [P1 + P2 + P3 + P8 + P9 + 1/2 (P6 + P7)], with P9 = 0

P<sub>ave</sub> II = 1/4 [P1 + P2 + P3 + 1/2 (P6 + P7)]

P<sub>ave</sub> III = 1/2 [P1 + P8]

P<sub>ave</sub> IV = 1/4 [P1 + P8 + P2 + 1/2 (P6 + P7)]

P<sub>ave</sub> V = 1/2 [P2 + 1/2 (P6 + P7)]

TABLE 3b - RIGID MODEL AT MIDPOSITION (7 1/4 IN. CLEARANCE)

Run	Event	Case Shown in Table 2	P1	P2	P3	P6	P7	P8	P <sub>ave I</sub>	P <sub>ave II</sub>
45	1		1.1°	0.85	0.4	0	0.6	0.35	0.4	0.65
67	1		3.3	4.8°	-	1.6	1.7	2.1	1.1	1.6
68	1		1.1°	-**	-	-	-	0.9	0.2	0.2
	2		4.0°	1.8	0.2	1.1	1.1	3.5	0.67	1.0
	3		3.5°	3.1	0.25	1.8	2.0	2.8	1.0	1.4
	4		3.0	4.4	1.0	0.7	7.1°	2.3	1.75	2.4
	5		1.85°	0.9	-	0.7	0.6	1.6	0.3	0.4
72	1		1.3	1.2	-	1.2	0.7	1.5°	0.35	0.5
	2		2.5°	2.3	1.0	1.0	1.4	1.3	0.4	0.65
73	1		2.2°	0.8	-	0.5	0.7	1.5	0.37	0.5
	2		1.1°	0.65	0.3	0.4	0.3	0.8	0.17	0.25
88	1		2.1°	0.25	-	0.6	0.15	1.3	0.30	0.45
	2		1.7	0.15	-	-	-	3.5°	0.58	0.30
92	1		1.65°	0.1	-	0.15	-	0.6	0.25	0.35
	2		1.9	1.5	-	1.0	0.9	2.0°	0.50	0.7
	3		1.85°	1.85°	-	0.2	0.9	1.1	0.45	0.6
	4		1.7	0.45	-	0.8	0.3	2.2°	0.4	0.45
93	1		1.4	1.25	0.15	2.2°	1.9	1.05	0.6	0.85
	2		2.55	4.3°	0.9	1.7	3.8	1.2	1.15	1.7
	3		0.8	1.45°	0.3	0.25	0.65	0.15	0.35	0.5
	4		0.8°	0.6	-	0.6	0.15	0.6	0.15	0.2
	5		1.9°	0.9	0.25	0.5	0.7	0.8	0.30	0.45

\*\* Values too small to read.

TABLE 3c - RIGID MODEL AT HIGH POSITION (10 1/4 IN. CLEARANCE)

Run	Event	Case Shown in Table 2	P1	P2	P3	P6	P7	P8	P <sub>ave I</sub>	P <sub>ave II</sub>
131	1		2.8	3.0°	0.4	1.2	1.0	2.6	0.6	0.9
136	1		0.75	0.5	0.4	0.8°	-0.5	0.05	0.15	0.2
	2		1.9°	1.35	-**	0.8	-0.6	0.4	0.3	0.45
	3		1.4°	0.6	0.6	0.7	-0.5	1.0	0.2	0.35
	4		1.5	1.8°	0.5	1.0	0.8	0.6	0.5	0.8
	5	I	2.1°	1.1	0.6	0.9	-0.4	0.4	0.3	0.55
137	1		1.2°	1.0	0.3	0.7	0.2	0.85	0.2	0.35
	2		1.55°	0.5	-	0.3	0.2	0.4	0.25	0.35
	3	I	1.3°	0.6	0.3	0.6	0.3	0.65	0.25	0.35
142	1	I	2.1°	1.0	-	0.55	0.2	0.15	0.45	0.55
	2		1.2°	-0.3	-	0.05	-0.2	0.2	0.2	0.3
	3		1.5°	1.2	0.1	1.0	0.7	1.3	0.35	0.5
	4		1.0	0.2	-	0.3	0.1	1.1°	0.2	0.25
	5		0.7°	-0.4	-	0.2	-0.2	0.5	0.15	0.2
146	1		0.9°	0.8	0.3	0.25	0.45	0.1	0.2	0.3

\*\* Values too small to read.

Figure 3d- Elastic Model at Midposition

Run	Event	Case Shown in Table 2	P1	P2	P3	P6	P7	P <sub>ave</sub>
251	1	I	2.7*	1.3	1.0	2.1	1.35	0.8
	2		0.7*	0.15	0.1	0.15	0.05	0.17
	3		1.85*	1.25	0.2	1.75	0.9	0.45
252	1		2.4*	0.8	0.35(-1.2)	0.8	0.8	0.6
	2		3.1*	1.5	0.6	0.9	0.9	0.75
	3		1.15*	0.3	-0.4	0.05	0.25	0.35
253	1	I	3.4*	1.2	0.1	0.65	0.75	0.95
	2		1.5*	1.1	0.5	1.0	0.6	0.45
	3		1.85*	0.85	0.75	0.7	0.4	0.5
	4		1.2*	0.65	0.65(-0.5)	0.5	0.3	0.3
256	1		3.1	2.95	0.2	4.3*	1.25	0.95
	2		0.7*	0.5	0.05	0.35	0.25	0.25
257	1		1.75*	1.2	0.5	1.0	1.6	0.85
258	1		2.5*	1.1	0.35	1.75	1.1	0.65
	2		2.9*	1.15	0.45	0.95	0.9	0.7
	3		3.6*	2.2	0.5	3.2	1.7	1.0
	4		2.0*	0.85	0.3	1.25	0.8	0.55
	5		3.2*	1.85	0.75	1.25	0.8	0.85
	6		2.5	2.25	0.9	2.15	2.9*	1.3
259	1		2.5	2.15	0.4	3.8*	1.85	1.2
	2		2.1*	1.25	1.15	1.2	1.0	0.75
	3		1.9*	1.25	0.85(-2.2)	1.3	1.0	0.5
	4		2.55	3.2*	0.9(-1.2)	2.3	0.85	1.45
264	1		1.85*	1.4	0.5	1.5	1.45	0.55
	2		1.3*	0.4	-0.4	0.4	0.2	0.35
	3		1.25	0.65	0.15	1.5	1.8*	0.55
	4		2.25*	0.5	0.05	0.1	0.2	0.55
	5		1.0*	0.45	0.05	0.3	0.25	0.25
	6		3.0*	0.75	0.45	0.9	0.4	0.7
	7		1.0	1.15	-0.55	1.0	1.35*	0.5

TABLE 3e - ELASTIC MODEL AT LOW POSITION

Run	Event	Case Shown in Table 2	P1	P2	P3	P6	P7	P <sub>ave</sub> II
317	1		1.2*	0.25	0.15	0.2	0.1	0.27
	2		1.5*	0.25	0.05	0.3	0.1	0.35
325	1		1.2*	0.15	0.05	0.1	Missing	0.25
	2		1.4*	0.2	0.05	0.1	0.25	0.37
	3		1.8*	0.15	0.05	0.15	0.25	0.45
	4		1.6*	0.7	0.05	0.6	0.6	0.45
	5		2.1*	2.0	0.35	1.5	1.45	0.67
	6		3.1*	0.7	0.25	0.8	0.6	0.7
	7	I	3.5*	1.3	0.7	1.5	1.45	0.87
	8		1.5*	0.3	0.1	0.2	0.25	0.4
	9		1.0	1.2*	0.15	0.4	0.3	0.3
	10		2.75*	0.65	0.1	0.65	0.4	0.95
	11		3.15*	1.5	0.9	1.5	2.4	0.8
327	1		1.9*	1.4	0.35	0.6	0.4	0.45
	2		0.75*	0.25	0.05	0.05	0.05	0.2
	3		3.5*	0.5	1.0	0.8	0.4	0.87
	4		2.8	3.6*	0.2	2.35	1.4	1.35
	5		1.2	0.6	0.2	1.25*	0.8	0.5
	6		1.1	0.7	0.3	1.35*	0.5	0.7
331	1		2.8*	0.3	0.4	0.45	0.4	0.7
	2		2.9*	0.5	0.3	0.65	0.7	0.7
	3		2.5*	0.5	0.1	0.6	0.4	0.65
	4		1.4*	0.6	0.55	0.55	0.45	0.4
334	1		2.75	2.35	0.3	1.85	2.8*	0.9
	2		3.3	2.2	0.9	4.6*	1.85	1.6
	3		2.3	1.85	0.7	2.3	2.35*	0.95
	4		3.2*	1.75	0.35	1.5	1.45	0.8
349	1		3.5*	0.7	0.1	0.6	0.65	0.87
	2		3.6*	1.5	0.15	1.1	0.85	0.87
	3		2.25	2.6	0.55	5.3*	2.2	1.85
	4		1.85*	0.65	0.1	1.0	0.67	0.47
	5		1.7*	0.3	-0.4	0.3	0.2	0.4
352	1		3.6	2.7	0.8	4.6*	2.8	0.95
	2		1.0	1.7	0.6	3.95*	0.5	0.95
359	1		3.25	1.2	1.5	3.9*	1.1	1.3
	2		2.2	1.6	1.55	2.9*	2.4	0.9
	3		3.35*	1.4	0.3	1.2	0.85	0.8

Figure 3f - Elastic Model at High Position

Run	Event	Case Shown in Table 2	P1	P2	P3	P6	P7	P <sub>ave</sub> II
387	1	II	1.4	1.85	0.15	2.65*	0.8	0.7
	2	III	1.7	1.1	0.1	2.1*	0.8	0.8
	3		1.7*	0.7	0.1	1.2	0.9	0.45
388	1		1.9*	1.1	0.1	1.65	1.8	0.55
	2		2.45*	1.85	0.1(-0.9)	2.25	1.0	0.7
	3		1.55	0.65	0.2(-0.75)	1.9*	0.9	0.65
	4		1.6*	0.85	-0.2	1.4	0.85	0.45
391	1		1.25*	0.45	0.2	0.6	0.15	0.35
	2	I	2.9*	2.4	0.35	2.25	1.2	0.75
396	1		1.45*	0.8	0.1	0.7	0.35	0.4
400	1		0.7*	0.05	NIL	0.4	0.4	0.2
409	1		1.9*	0.3	0.1	0.6	0.2	0.5
	2		3.35	2.4	0.6	3.8*	1.2	0.85
411	2		2.25*	1.3	0.1	1.1	1.3	0.55
412	1		2.4*	0.75	NIL	1.0	1.2	0.6
	2		2.5*	2.1	0.5	1.9	1.4	0.65
	3		2.4*	2.1	0.45	2.4*	1.0	0.9
	4		2.4*	0.95	0.1	1.35	0.95	0.6
	5		2.6	1.90	0.5	3.6*	2.6	1.1

TABLE 3g - P<sub>max</sub>/P<sub>ave</sub> (SAMPLES)

Run	Event	Model	Position	T <sub>w</sub> sac	V <sub>k</sub> knots	P <sub>max</sub>		P <sub>ave</sub> I	P <sub>ave</sub> II	P <sub>max</sub>	P <sub>max</sub>
						P1	P2			P <sub>ave</sub> I	P <sub>ave</sub> II
9	9	Rigid	Low	1.4	0.66		4.1	0.95	1.25	4.32	3.28
12	2	↓	↓	1.4	1.98	6.3		1.05	1.65	6.00	3.82
31	3			1.71	1.32	3.1		0.60	0.95	5.17	3.26
39	3			1.71	1.98	2.7		0.50	0.70	5.41	3.86
40	2			Low	1.71	2.64		4.0	1.30	1.75	3.08
67	1		Mid	2.0	1.65		4.6	1.10	1.60	4.18	2.88
68	2		Mid	2.0	1.98	4.0		0.67	1.00	6.00	4.00
	3		Mid			3.5		1.00	1.40	3.50	2.50
142	1	Rigid	High	1.71	1.98	2.1		0.45	0.55	4.67	3.80
251	1	Elastic	Mid	1.71	1.32	2.7			0.80		3.38
258	5	↓	Mid	1.71	1.98	3.2			0.85		3.77
259	4		Mid	1.71	2.64		3.2		1.45		2.21
327	4		Low	1.71	1.98		3.6		1.35		2.67
412	3	Elastic	High	2.0	1.98	2.4			0.90		2.67

Note: If other pressures are zero except p<sub>max</sub>, then p<sub>max</sub>/P<sub>ave</sub> I = 6.0 and p<sub>max</sub>/P<sub>ave</sub> II = 4.0. In other words, at most, p<sub>max</sub> is six times P<sub>ave</sub> I and four times P<sub>ave</sub> II. However, if negative pressures occur at the same time that p<sub>max</sub> occurs, then p<sub>max</sub>/P<sub>ave</sub> I > 6.0 and p<sub>max</sub>/P<sub>ave</sub> II > 4.0.

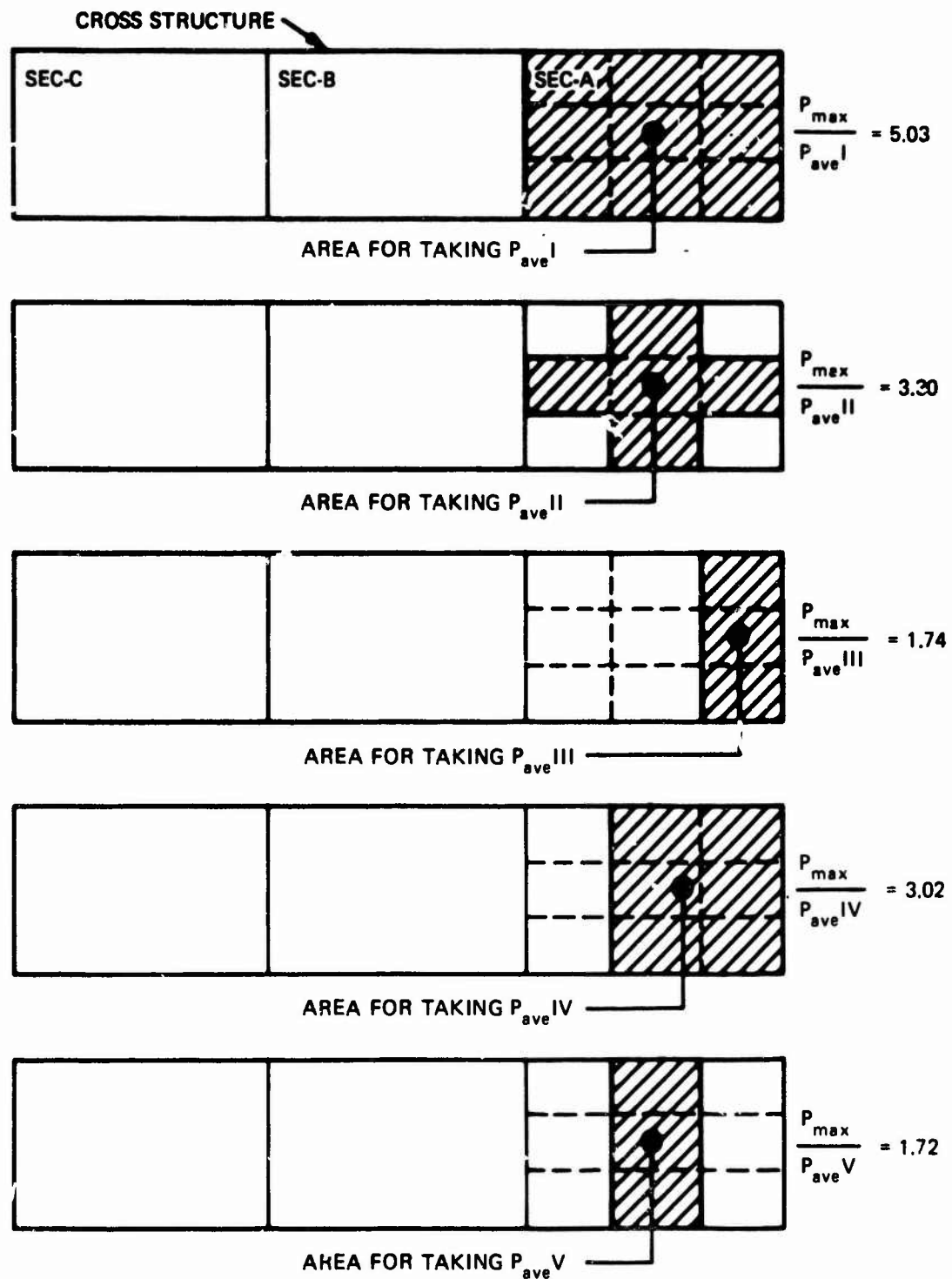


Figure 7 - Area Used to Take Average Impact Pressures at Forward Section of Cross Structure

( $P_{max}$  is the maximum peak pressure within the averaging area; values given for  $P_{max}/P_{ave}$  are the mean values for Runs 37, 39, and 40 given in Table 3a.)

(a) Area I > Area II gives  $p_{ave} I < p_{ave} II$

(b) Area IV > Area III or V gives  $p_{ave} IV < p_{ave} III$  or V

The information on slamming pressure distribution provided from the results of these tests offers some guidance for design consideration that can be summarized as follows:

1. The highest peak pressure occurs at the center forward end of the cross-structure bottom.
2. Pressures at the sides are usually smaller than at the centerline.
3. The most severe slamming occurs at the foremost portion of the cross-structure bottom. There is little slamming at the LCG of the model. Similarly, slamming pressures at the aft end of the cross-structure bottom are small or insignificant. (On rare occasions the slamming pressure at the aft end can be quite large, but it is still less than the pressure at the forward end.)
4. The average pressure over the entire area of the forward section is less than about one-fourth the localized highest peak pressure in that area; see Figure 7 and Table 3.

Figures 8 and 9 illustrate the application of these design guidance considerations as used by the design agent to determine load criteria for strengthening the bottom of the HAYES cross structure. Figure 8 depicts the relative pressure intensity factor versus longitudinal location or ship station. Figure 9 shows the maximum equivalent static pressure acting over an area of the bottom of the cross structure versus the number of plate areas considered. Based on the information provided in Figures 8 and 9, the reinforced HAYES cross-structure bottom grillage was designed to withstand a static pressure of 50 psi at Station 3 over an area of approximately 300 ft<sup>2</sup>. This criterion for pressure was linearly reduced from 50 psi at Station 3 to 10 psi at Station 14, and was held constant at 10 psi aft of Station 14.

#### **EFFECT OF DEFORMABILITY OF IMPACT SURFACE**

A close examination of Figure 6 shows that the k values obtained from the equation  $p_{max} = k \rho V_a^2$  are generally lower for the deformable body impact than for the rigid body impact. But there are a great number of exceptions; likewise, the reduction in peak pressure due to deformability of the impact body is not very obvious. The difference in rigidity (or flexibility) of two types of models (1/4-in. plate for the "rigid-body" against 1/32-in. plate thickness for the "deformable-body" model) was apparently too small to enable differences

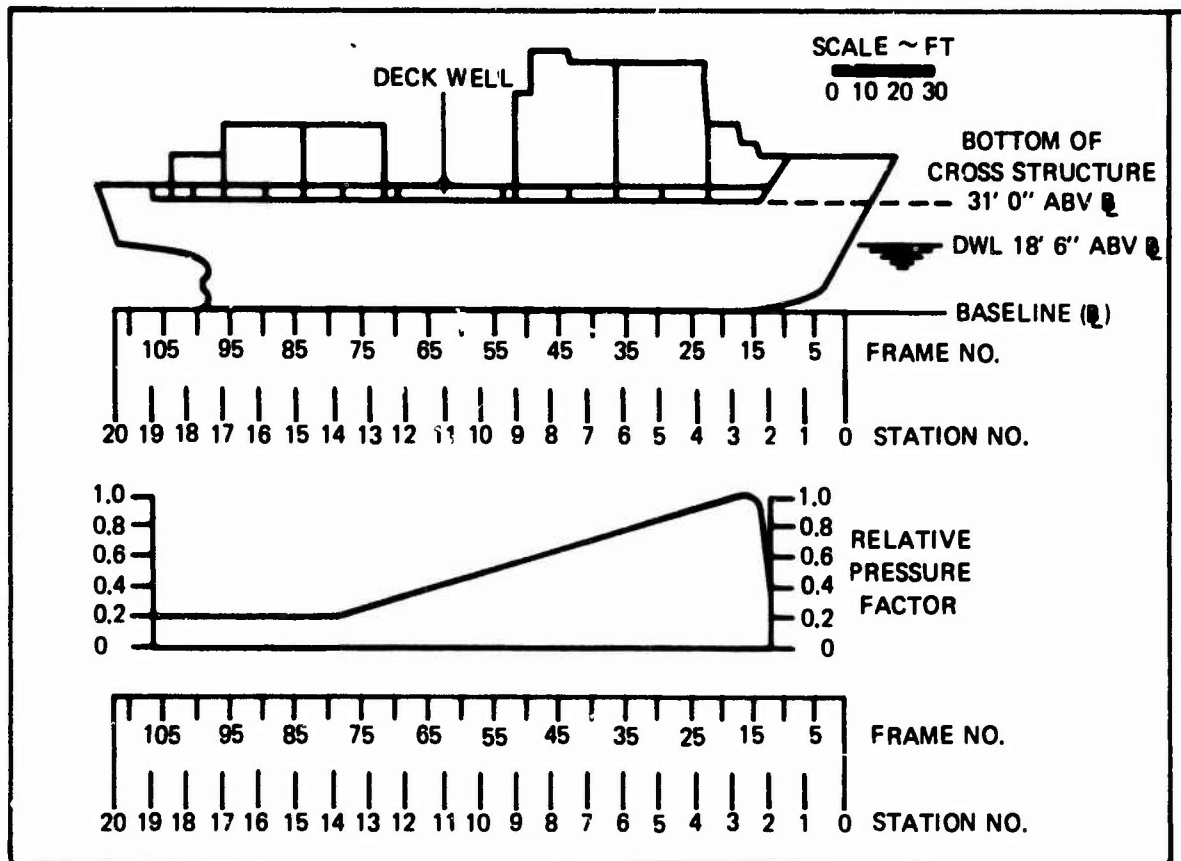


Figure 8 - Relative Wave Impact Pressure on Bottom of Cross Structure versus Ship Station

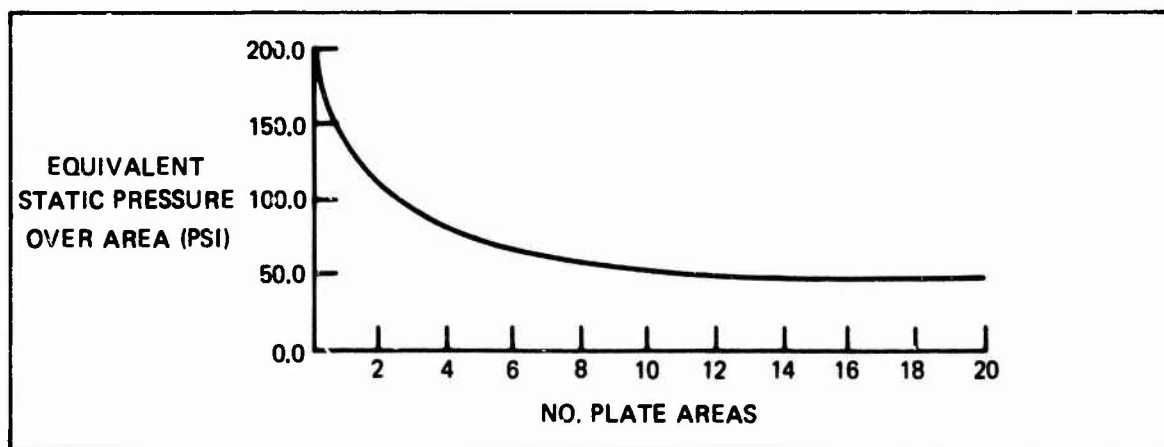


Figure 9 - Maximum Pressure versus Wave Impact Surface Area  
(One plate area is about 16 ft<sup>2</sup>; 22 x 96 in. fwd of Frame 24 and 24 x 96 in. aft)

to be measured for small values of the impact pressures. In addition, rigid and elastic models were tested in separate runs, and that made comparisons more difficult.

Figure 10 shows that the deformability of the impact surface also affects the pressure time histories. The effect of deformability is indicated in the figure by the differences of the pressure time histories of the pressure records of Run 37 for the 1/4-in.-plate rigid model and of the pressure records of Run 325 for the 1/32-in.-plate deformable model. These results also mean that the deformability affects the pressure time histories as well as the peak impact pressures. This phenomenon is discussed mathematically and in more detail elsewhere.<sup>1</sup>

#### **EFFECTS OF CROSS-STRUCTURE CLEARANCE, SHIP SPEED, WAVE CELERITY, AND WAVE HEIGHT**

Although the experiments were conducted under regular wave conditions, records indicated that the wave surface was distorted and hence somewhat irregular during a series of slamming events. Usually more than ten slamming events were recorded during each run, but none of them was identical. It was therefore very difficult to make a systematic analysis of all the records. Those considered applicable were selected for the comparison of measured and predicted impact pressures. Thus in this section, only general conclusions have been drawn from observations and experimental records.

Changes in cross-structure clearance, ship speed, wave celerity, and wave height can affect ship motions and thus the value of the impact angle, the impact velocity, and the impact pressure. Changes in ship headings were not investigated.

The increase in cross-structure clearance above the water surface reduced the frequency of impact, but it increased the pitch and heave motions of the model. Because of the increase in ship motions, no obvious reduction of impact pressure, solely attributable to the higher clearance can be determined from the records. Generally, the higher clearance increased the impact angle (see Table 2) and thus is expected to reduce the impact pressure for the same impact velocity. However, many test runs (see Table 2) showed that the impact angle was independent of the clearance. In general, there was a reduction of impact pressure for the higher clearance, but it is difficult to define a specific percentage reduction value from the results.

The increase in ship speed increases the frequency of encounter of the wave by the ship. It is generally known that if the frequency of encounter becomes synchronized with the natural pitch and/or heave frequencies of the ship, it produces the highest pitch and/or heave motions. This causes an increase in impact velocity and thus an increase in impact pressure.

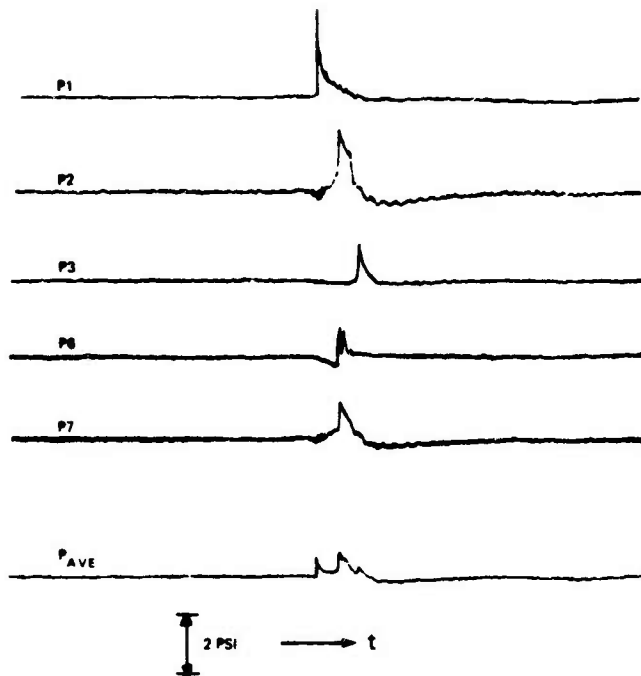


Figure 10a - Rigid Model, Run 37

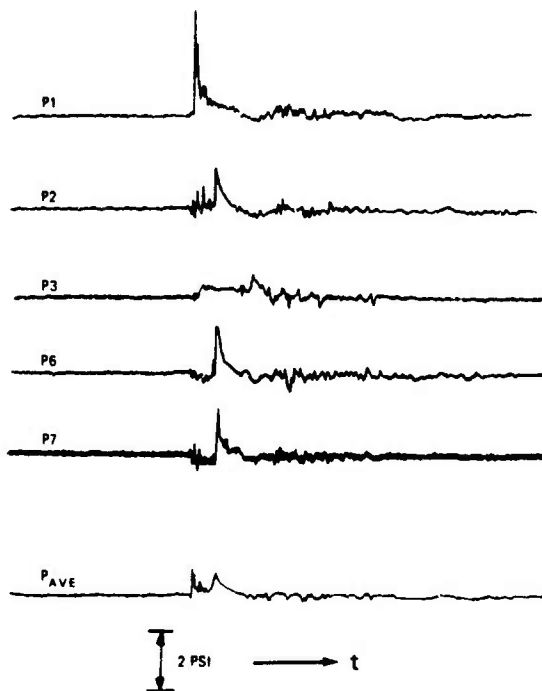


Figure 10b - Elastic Model, Run 325

Figure 10 - Impact Pressure Records

For a particular ship speed and heading, it is wave celerity which determines ship-to-wave frequency of encounter; in turn, this also affects ship motions, impact velocity, and impact pressure. The effect of wave height on the impact pressure is obvious, that is, higher waves produce higher impact velocity in the ship slamming area, and thus higher impact pressure. This higher impact velocity is produced partly by the wave itself and partly by the increase in ship motion.

### ADDITIONAL EXPERIMENTAL FINDINGS

Some additional findings were collected from the observations made during the conduct of the experiments and the analyses of resulting records:

1. Slamming occurs more frequently when the combined pitch and heave motions of the model at the bow are over 90 deg out-of-phase with the wave surface. This finding applies even in a relatively moderate sea with the wave amplitude less than the cross-structure clearance above a calm water surface.
2. Impact pressures caused by wave slap were found to be insignificantly low and almost immeasurable for the models tested. Here wave slap is defined as the impact of a wave crest on the bottom of the cross structure without any ship motions.
3. When the model was towed astern into drydock (i.e., towed backwards) to simulate following seas after each run, slamming occurred infrequently and insignificantly because of small ship motion.
4. As shown in Table 2, the highest peak pressure reading was about 7 psi (e.g., Run 218). The 7-psi pressure for the model is equivalent to 150 psi for the ship. Before a motion-mitigating hydrofoil was installed on HAYES, some readings during her sea trials registered pressures as high as 200 psi on the bottom of the forward cross structure. Therefore, the recorded pressures from the model tests are considered realistic.
5. As expected, the forward half of the forward cross-structure elastic model section (1/32-in. bottom plating) was dished in with a 1/4-in. permanent set. Of course, such severe slamming conditions could possibly be avoided during actual ship operation by slowing down and/or changing course to reduce the severity of the motions.
6. The highest peak pressure (2.2 psi) registered by the pressure gage that had been installed on the front vertical bulkhead of the cross-structure model is equivalent to 46 psi on a full-scale ship. This is twice the stagnation pressure, i.e.,

$$p = 2(1/2 \rho V^2) \text{ (in pounds per square foot)}$$

$$V = V_h + V_w$$

(10)

The factor of 2 that is needed in this equation is attributed to the sudden application of the impact load.

7. Since the front bulkhead is open to the impact of the wave, its shape should be sloped or, preferably, curved horizontally and/or longitudinally where practicable in order to reduce the wave impact load.\*

8. The largest pitch angle recorded was about 26 deg peak-to-peak. The largest heave recorded was 16 in. peak-to-peak, or 28 ft for a full-scale ship. These values generally compare with those recorded during the recent sea trials of HAYES.

9. Slamming generally occurs when the bow is fully depressed (i.e., pitch angle is approaching its maximum bow-down attitude and pitch velocity is approaching zero) and heave velocity is approaching its maximum (i.e., heave displacement near zero) against the wave surface. The point of impact can be anywhere on the wave surface, but the most frequent and severe impacts occur at the forward section of the cross structure. (This phenomenon was also noted in the HAYES slamming records.)

#### CONSIDERATIONS FOR THE PRACTICAL STRUCTURAL DESIGN OF CROSS STRUCTURE IN THE SLAMMING AREA

The present series of investigations now makes it possible to provide some design load criteria for the cross structure in the slamming area. Only the local slamming loads are considered. Determination of other types of loadings, such as longitudinal hull bending wave and vibratory loads, is not within the scope of the present study.<sup>9,10</sup>

This section provides a method for determining the slamming pressure (or load) and its distribution in the slamming area of the cross structure.

---

\* The 46 psi noted above could be reduced to perhaps 20 psi if the front bulkhead were curved 2 to 3 deg horizontally.

<sup>9</sup>Dinsbacher, A.L. et al., "Model Test Determination of Sea Loads on Catamaran Cross Structure," NSRDC Report 2378 (May 1967).

<sup>10</sup>Lankford, B.W., Jr., "The Structural Design of the ASR Catamaran Cross Structure," Naval Engineers Journal, Vol. 79, No. 4 (Aug 1967).

## DETERMINATION OF PEAK IMPACT PRESSURE

In determining a predicted value for the peak impact pressure, the impact velocity and the impact angle must be obtained either from information on ship motions and waves or from direct measurement. The highest slamming loads are generated in head seas; the maximum pitch and heave motions usually occur under such conditions.

At the present time, the most reliable method for obtaining such information as pitch and heave and their phase angles with the wave is by means of a seakeeping test of a model or by sea trials. However, motion prediction methods are also available.<sup>11,12</sup>

The seakeeping test (or motion prediction method) usually does not include measurements of slamming pressures or loads. However, when ship motion data are available, they enable slamming pressures to be determined, e.g., by Equation (7) or (9). Equation (7) requires knowledge of the heave velocity  $V_{hea}$ , the pitch velocity  $V_p$ , the vertical velocity of wave surface  $V_{wav}$ , the pitch angle  $\theta_p$ , and the wave slope  $\theta_w$ . These quantities can be determined by trigonometrical equations if the motions are assumed to be sinusoidal. The maximum impact pressure at the centerline of the cross structure can thus be determined by Equations (1) through (5). As generally indicated in Table 3, the impact pressure distribution athwart to the cross structure may be approximated by a parabola with the peak at the center and 70 percent of the center value at the sides. A typical pressure distribution along the centerline of the cross structure is illustrated in Figures 8 and 10. Typical examples of the ratios of maximum to average pressures for various portions of the underside structure are shown in Figures 7 and 9.

## STRUCTURAL RESPONSE

As demonstrated by Chuang,<sup>1</sup> the structural response to slamming can be determined mathematically. However, in view of the present state-of-the-art, it is quite satisfactory to assume that the slamming loads are to be applied quasi-statically. In other words, the cross structure will be relatively rigid for most practical design uses, and so it is reasonable to assume that the load is applied quasi-statically to the rigid-body impact area of the cross-structure bottom.

---

<sup>11</sup>Lee, C.M. et al., "Prediction of Motion and Hydrodynamic Loads of Catamarans," *Marine Technology*, Vol. 10, No. 4 (Oct 1973).

<sup>12</sup>Hadler, J.B. et al., "Ocean Catamaran Seakeeping Design, Based on the Experience of USNS HAYES," *Transactions Society of Naval Architects and Marine Engineers*, Vol. 82 (1974).

Once he has determined cross-structure bottom slamming loads, load distributions, and method of application of loads, the designer can complete the design of plate, panel, and grillage structure in the usual manner. He may design the structures either conservatively or liberally, guided by his own judgment, by owner's specifications, by rules and regulations of the classification societies, and by design manual, design data sheets, design technical practices, etc.

## SUMMARY AND CONCLUSIONS

Earlier NSRDC studies on slamming involved drop tests of two- and three-dimensional monohull models.<sup>1,13</sup> The present study covers the slamming of the cross-structure bottom of a conventional catamaran model.

Two catamaran cross-structure models were utilized; one had 1/4-in. aluminum flat plate as the impact surface and the other had 1/32-in. aluminum flat sheet. Experiments were conducted in regular waves with lengths from 10 to 30 ft, heights up to 2 ft, and clearances of 4 1/4, 7 1/4, and 10 1/4 in. beneath the cross structure.

The objectives of the investigation were: (1) to establish levels for realistic values of slamming loads and load distributions acting on a rigid and a deformable bottom of a catamaran cross structure, (2) to verify a method for predicting cross-structure bottom slamming pressure by comparing calculated values with those obtained in model experiments and full-scale trials, and (3) to provide design guidance for determining the scantlings of the cross structure in the slamming area.

Two methods are available for predicting the slamming pressures. Both are based on the relative velocity of the impact surface of the moving body and the wave surface. However, the first method used the movement of the wave surface and the second employs the orbiting velocity of water particles. Both methods predict the pressures with reasonable accuracy. Since irregularity of the wave surface was indicated in the experimental records, the first method was considered more applicable for comparisons of experimental and predicted results.

On the basis of this series of experimental investigations of conventional catamaran slamming, the following conclusions have been drawn:

1. The most frequent slamming and highest peak pressures usually occur at the forward end and on the center of the cross structure. Slamming occurrences were much less

---

<sup>13</sup>Ochi, M.D. and J. Bonilla-Norat, "Pressure-Velocity Relationship in Impact of a Ship Model Dropped onto the Water Surface and in Slamming in Waves," NSRDC Report 3153 (Jun 1970).

frequent at amidship and at the aft end. The agreement between experimental results and predicted values of the pressures were considered very good, especially in view of the many uncertainties involved in the measurements of the wave properties and their relation to ship motions, velocities, impact angles, etc. (see Figure 6).

2. Obviously, the highest average slamming pressure over a large area is less than that at the localized area. For example, the peak pressures measured by the gages at the forward panel of the cross structure were two to six times the average pressures over the panel (see Figure 7 and Table 3). The average pressure also depends on the impact angles; i.e., for two identical sizes of impact areas, the difference between peak and average pressures is greater for the larger impact angles.

3. The deformable impact surface relieves slamming pressure. However, the differences in pressure between the tested "rigid" and "deformable" aluminum models were too small for an objective comparison. The peak pressure of the deformable impact surface was usually less than that registered for a comparable rigid surface impact. In any case, for the practical design of conventional steel structures, it is reasonable to assume that the slamming load is quasi-static and independent of the deformability of the impact surface.

4. Higher cross-structure clearance over the water surface reduces the frequency of slamming and slamming pressure. Experiments at three different heights did not clearly indicate the percentage of reduction of slamming pressure associated with the higher clearances.

5. Ship speed and wave celerity affect ship motions. When the ship is at a synchronous speed (i.e., the period of wave encounter is approximately equal to the natural pitch and/or heave periods), its motions per foot of wave height increase and thus the slamming pressure is expected to be larger than at nonsynchronous speeds.

6. Higher waves generate higher slamming pressure partly because of increased wave height and partly because of larger ship motions resulting from the increased wave height.

7. A following sea causes insignificant slamming because of reduced ship motions.

8. The predominant source of severe slamming is ship pitch and heave motions rather than waveslap. If ship motions can be reduced by changing ship speed or course, slamming intensity will be reduced.

9. The general procedures for the design of the cross structure in the slamming area are (a) to determine ship motions and velocities from seakeeping model tests or as described by Lee<sup>11</sup> and Hadler,<sup>12</sup> (b) to determine impact pressure by the method given in the report, (c) to determine pressure distribution in the slamming area as suggested in the report, (d) to apply load quasi-statically, and (e) to design structures by the usual design method.

The prediction method developed herein was used to obtain results that could be compared with the slamming experienced by HAYES during sea trials. Considering the many variables involved in the predictions, calculated values are considered to be in good agreement, with the HAYES results.

### ACKNOWLEDGMENTS

This project was a team effort that involved many people. The cross-structure models were designed by Messrs. L.M. Buiger and A.R. Synstad of the Central Instrumentation Department. Messrs. D.T. Milne and S.E. Dawson, also of the Central Instrumentation Department, supervised development of the instrumentation systems used to collect model test and HAYES trial data, respectively. The authors gratefully acknowledge their helpful assistance and valuable suggestions.

The support of Structures Department personnel from the Advanced Ship Division, particularly Mr. A.L. Dinsenbaeher who is the coordinator of research on catamaran structures, is greatly appreciated.

Since the series of fundamental research studies on slamming is nearly complete, it is appropriate to take this opportunity to express thanks to Dr. W.W. Murray and Mr. A.B. Stavovy for their continuous support and all possible assistance for over a decade.

**APPENDIX A**  
**ANALYSES OF HAYES SEA TRIAL CROSS-  
STRUCTURE SLAMMING DATA**

Full-scale trials were conducted near the end of the HAYES first winter of operation in the North Atlantic (1972) when it became apparent that there were problems of cross-structure slamming. It was fortunate that the HAYES data provided information needed for the determination of cross-structure slamming pressure by Method I. To verify the usefulness of the prediction method, 12 slamming occurrences, obtained during two trial runs when the slamming was most severe, were analyzed and the values predicted by Method I were compared with the full-scale results. These two runs were conducted before the installation on HAYES of a forward foil to reduce slamming. Hadler et al.<sup>12</sup> provide detailed information on sea trials, gage locations, etc.

Data used as input for the slamming pressure prediction program are summarized in Table A.1, and the calculated k values (or pressure intensity factor) determined from the sea trials are shown in Figure A.1. Considering the many variables involved in the calculations, the 3-dimensional slamming predictions shown in the figure are considered to be in good agreement with results derived from HAYES trial data.

TABLE A.1 - SUMMARY OF HAYES SLAMMING DATA AND COMPUTER RESULTS

Event Hr, min, sec	Case	$\theta_p$ deg	Recd $p_t$	$\theta_{av}$ deg	$\theta_r$ deg	$V_{has}$ fps	$V_{yaw}$ fps	$V_p$ fps	$V_n$ fps	$\xi$ deg	Calc $p_t$	k (Computer)		
												Eq(1),(2)	Each	Mean
A. PHASE III, RUN 11-23-8 (NO FOIL)														
16,52,49	I	-5.52	95	-3.17	4.0	-	3.52↓	10.5↓	7.04	4.64	40	0.409	0.964	0.825
	II					3.01↓	3.52↓	8.8↓	8.34	4.64	57	0.409	0.686	0.413
16,56,12	I	-5.33	38	-1.58	0.0	-	1.75↓	8.5↓	8.80	3.75	47	0.515	0.413	0.363
	II					4.07↓	1.75↓	5.45↓	7.81	3.75	63	0.515	0.313	0.363
16,59,54	I	-5.43	68	-2.13	2.01	-	2.3↓	10.2↓	7.96	3.86	63	0.498	0.522	0.476
	II					4.58	2.3↓	8.8↓	9.13	3.86	83	0.498	0.410	0.476
17,00,38	I	-2.91	115	-2.78	2.82	-	3.09↓	11.0↓	7.93	2.82	87	0.682	0.920	0.780
	II					4.58↓	3.09↓	8.0↓	9.50	2.82	124	0.682	0.640	0.780
17,00,43	I	-4.46	70	-1.8	0.87	-	2.00↓	9.05↓	7.08	2.78	70	0.703	0.700	0.700
	II					4.97↓	2.00↓	4.10↓	7.10	2.78	70	0.703	0.700	0.700
17,14,01	I	-4.66	55	-1.22	1.22	-	1.35↓	13.9↓	12.81	3.65	108	0.530	0.175	0.174
	II					6.03↓	1.35↓	7.96↓	12.88	3.65	170	0.530	0.172	0.174
B. PHASE III, RUN 11-23-14 (NO FOIL)														
21,35,52	I	-5.44	77	-3.36	1.41	-	4.36↓	11.8↓	7.52	2.51	87	0.774	0.684	0.566
	II					4.2↓	4.36↓	9.4↓	9.32	2.51	134	0.774	0.446	0.566
21,35,57	I	-4.36	57	0	0	-	0	7.1↓	7.12	4.36	44	0.437	0.566	0.567
	II					7.1↓	0	0	7.10	4.36	44	0.437	0.509	0.567
21,37,28	I	-2.6	27	-2.8	0.20	-	3.56↓	7.2↓	3.65	0.28	15	0.548	1.02	0.834
	II					5.9↓	3.56↓	2.23↓	4.58	0.28	23	0.548	0.648	0.834
21,44,03	I	-6.3	85	0	3.02	-	0	14.8↓	14.87	8.98	115	0.282	0.193	0.197
	II					9.7↓	0	4.9↓	14.81	8.98	111	0.282	0.200	0.197
21,45,16	I	-5.72	46	-2.38	1.0	-	6.95↓	1.86↓	5.83	3.49	38	0.567	0.681	0.681
	II					9.84↓	0	20.8↓	20.77	8.63	171	0.199	0.175	0.181
21,47,56	I	-8.0	150	0	3.24	-	0	10.25↓	20.18	8.63	181	0.199	0.186	0.181
	II					9.84↓	0	10.25↓	20.18	8.63	181	0.199	0.186	0.181

NOTE: 1. For Case I  $V_p$  was measured at impact area. For Case II,  $V_p$  was calculated by  $\theta_p$  and  $V_{has}$  was measured at longitudinal center of gravity.  
 2. The recorded  $p_t$  is the maximum peak value among measured gage peak values.

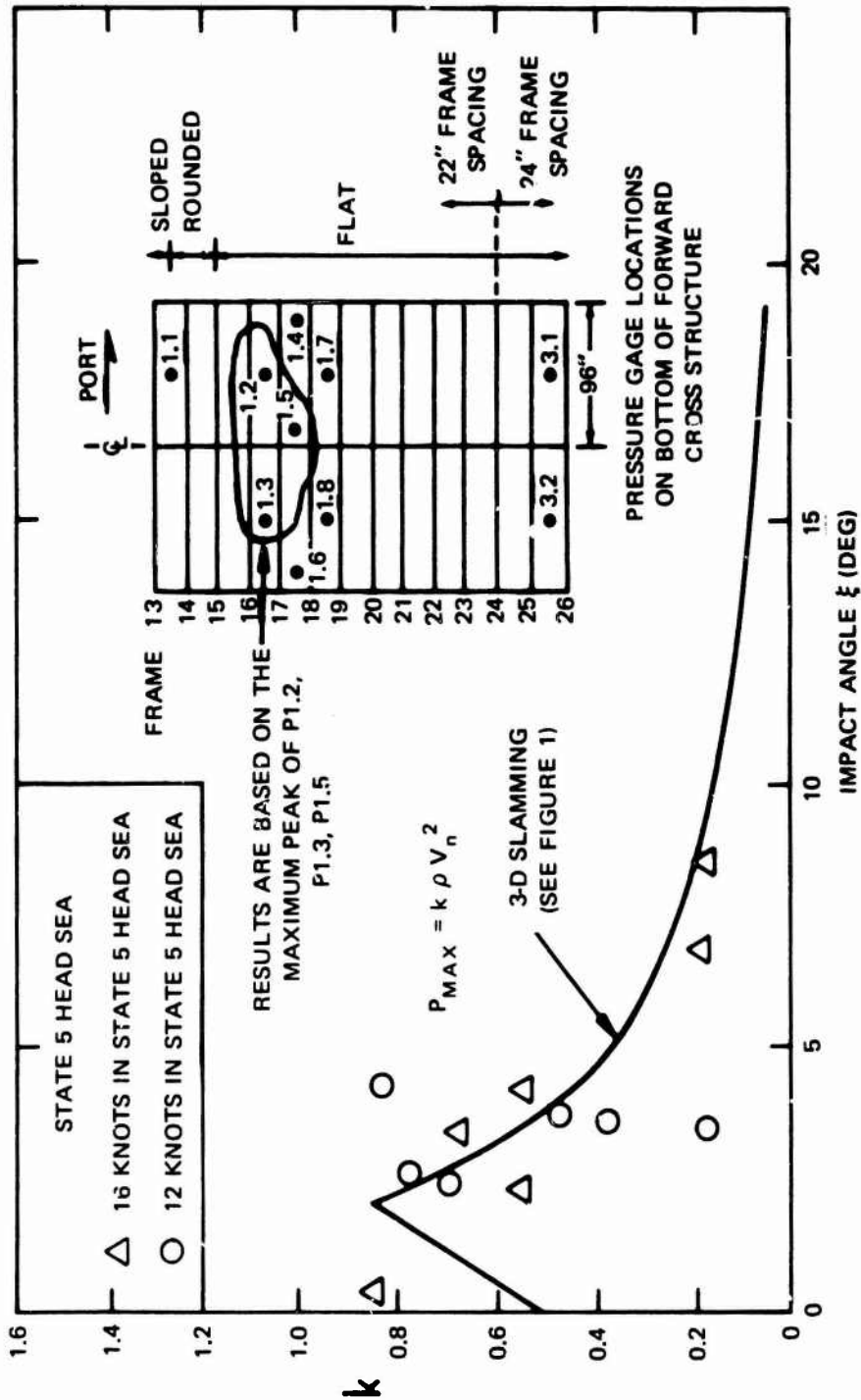


Figure A.1 — Predicted and Measured Peak Pressure Factor  $k$  versus Impact Angle for HAYES as Built

( $V_n$  is velocity normal to wave surface at impact and  $\rho$  is mass density of fluid)

## APPENDIX B METHODS OF DATA COLLECTION AND REDUCTION

### DATA COLLECTION

The data for each run were collected into four groups—each consisting of 14 channels. The first seven channels of each group were continuous through each run and they consisted of time (T), pitch angle (P), heave distance (H), wave height (W1), relative wave height (W2), acceleration (A), and slamming pressure at the front face of the cross structure (P14). The remaining seven channels were changed for each group. The first three groups corresponded to the three sections of the cross structure and the fourth group recorded the slamming pressures over its whole length. For the elastic models, for example, Group A recorded pressures at three points ( $P_1, P_2, P_6$ ), deflection (DA), stresses (SAF, SAS), and acceleration (AA); Group B recorded pressures at three points ( $P_2, P_4, P_5$ ), deflection (DB), stresses (SAF, SAS), and acceleration (AB); Group C recorded pressures at three points ( $P_2, P_4, P_5$ ), deflection (DC), and acceleration (AC); and Group D recorded pressures at seven points ( $P_1-P_7$ ). The locations of these gages are shown in Figure 5. Similar grouping was applied to data collection for the rigid models.

### DATA REDUCTION

Figure B.1 shows a portion of a record collected during the experiment. These records provided the information needed for the computer prediction of slamming pressure, namely:

Run No. — given.

Case No. — given.

TD — Pitch angle in degrees.

PNR — Recorded impact pressure in pounds per square inch.

WSD — Wave slope in degrees.

VHEA — Heave velocity in feet per second—from record.

VWAV — Vertical velocity of wave surface in feet per second.

VP — Vertical velocity (in feet per second) due to pitch.

The procedure for reducing the data is as follows. The time of impact is obtained by drawing a vertical line through the peak of a selected pressure time history and extending it through all channels to determine the related ship action.

The determinations of pitch, heave, and wave velocities from the experimental records are as follows:

1. Pitch Velocity (VP):

$$\text{From Figure B.2, the pitch velocity is } VP = \frac{\Delta P}{\Delta t} \cdot \text{cal} \cdot \frac{2\pi}{360} \cdot \ell$$

where  $\ell$  is the distance of pressure gage from the CG of the model, and cal is the test record calibration factor.

2. Heave Velocity (VHEA):

From Figure B.3, the heave velocity is:

$$VHEA = \frac{\Delta H}{\Delta t} \cdot \text{cal}$$

3. Pitch Angle (TD):

From Figure B.4, the pitch angle is:

$$TD = \theta_p \cdot \text{cal}$$

4. Wave Slope (WS):

Since the wave probe is located  $s$ -distance ahead of the impact point where pressure is measured, the impact point for the wave is recorded  $t(w)$  sec ahead of the impact line drawn on the record. As shown in Figure B.5,

$$t(w) = s/V(H)$$

where  $V(H)$  is the sum of the wave velocity and the model speed. The wave slope is then

$$WSD = \frac{\Delta W}{\Delta t} \cdot \text{cal} \cdot \frac{1}{V(H)} \left( \frac{360}{2\pi} \right)$$

Once the data were reduced, they were entered into the computer program, given in Table 1, for comparison with the levels predicted by the program.

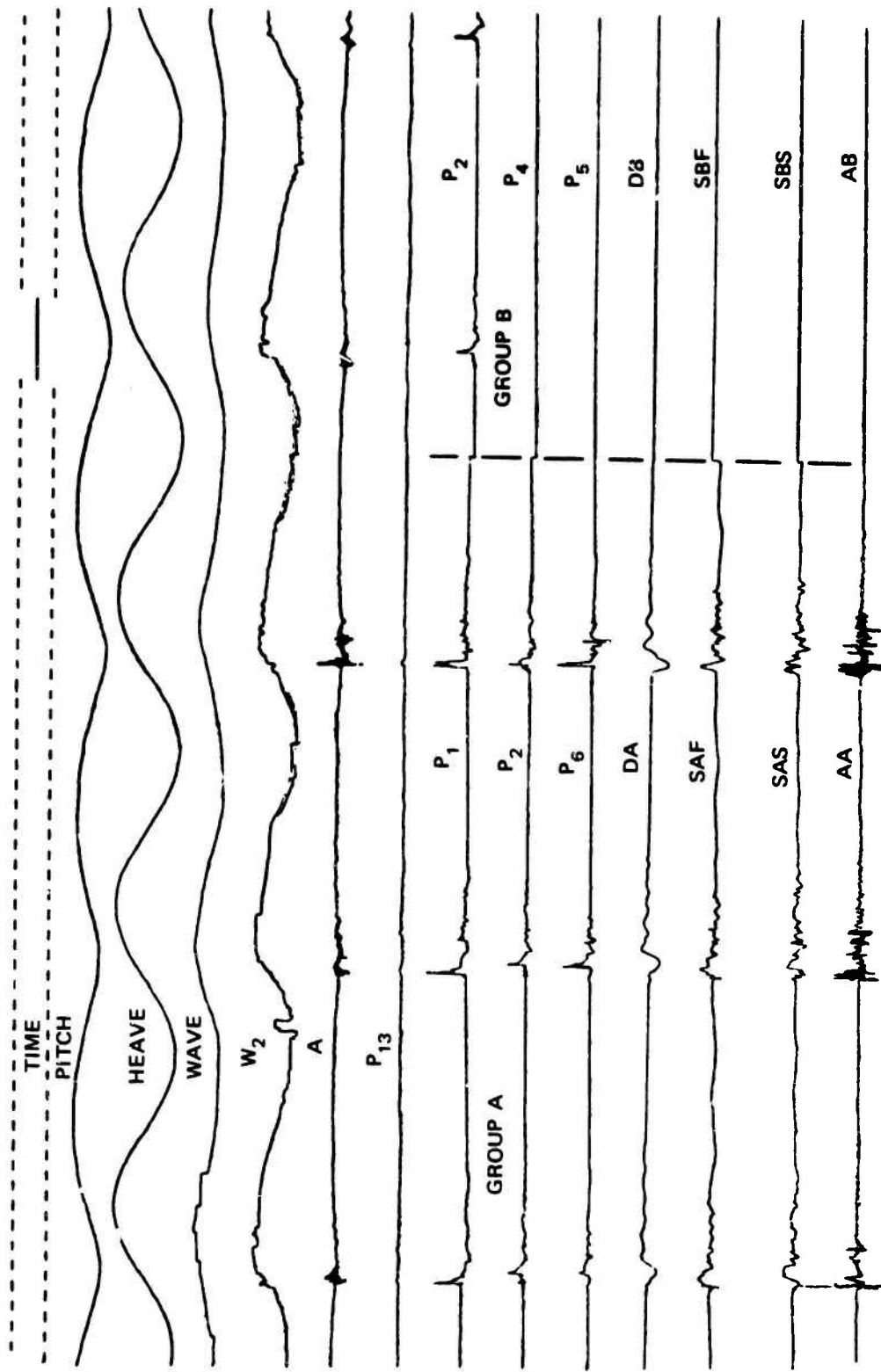


Figure B.1 - Sample Record for Elastic Model

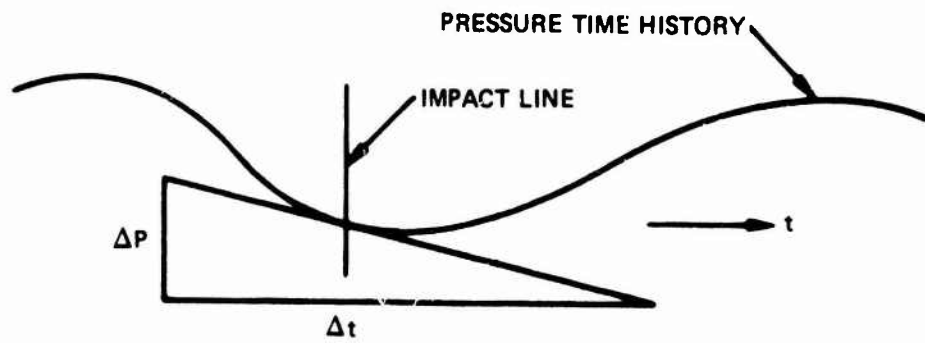


Figure B.2 – Determination of Pitch Velocity

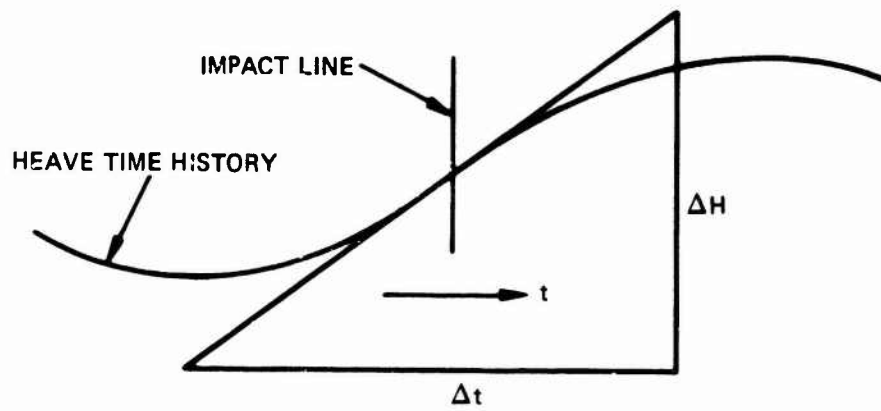


Figure B.3 – Determination of Heave Velocity

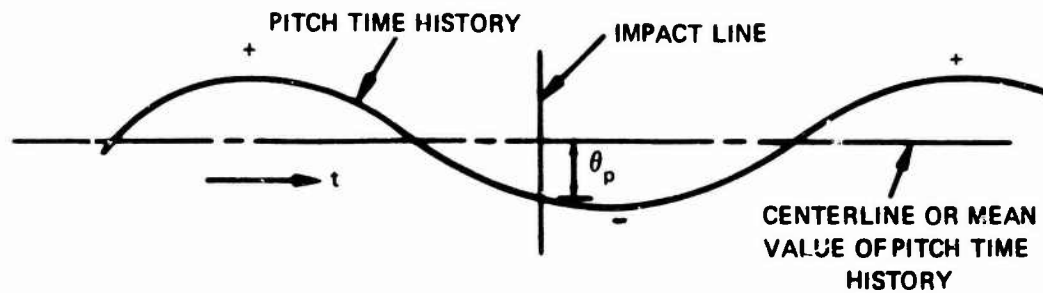


Figure B.4 – Determination of Pitch Angle

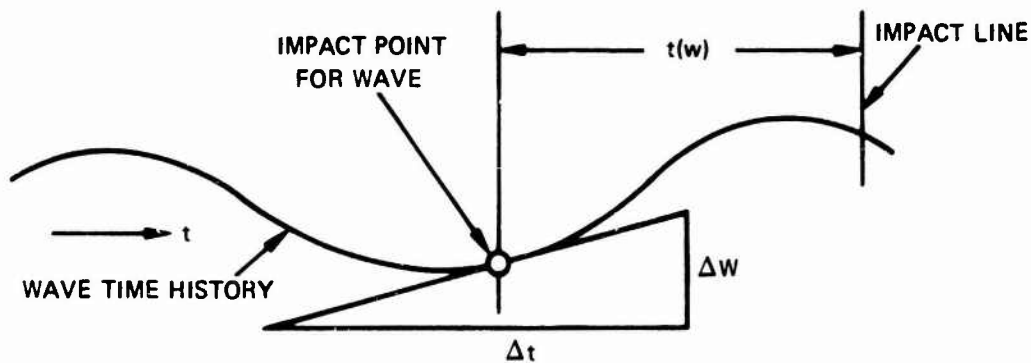


Figure B.5 – Determination of Wave Slope

## REFERENCES

1. Chuang, S.L., "Investigation of Impact of Rigid and Elastic Bodies with Water," NSRDC Report 3248 (Feb 1970).
2. Chuang, S.L., "Impact Pressure Distributions on Wedge-Shaped Hull Bottoms of High-Speed Craft," NSRDC Report 2953 (Aug 1969).
3. Chuang, S.L., "Design Criteria for Hydrofoil Hull Bottom Plating," NSRDC Report 3509 (Jan 1971).
4. Chuang, S.L., "Slamming Tests of Three-Dimensional Models in Calm Water and Waves," NSRDC Report 4095 (Sep 1973).
5. Wagner, V.H., "Über Stosz- und Gleitvorgänge an der Oberfläche von Flüssigkeiten," Zeitschrift für Angewandte Mathematik und Mechanik, Vol. 12, No. 4, pp 193-215 (Aug 1932).
6. Chuang, S.L., "Theoretical Investigations on Slamming of Cone-Shaped Bodies," Journal of Ship Research, Vol. 13, No. 4 (Dec 1969).
7. Chuang, S.L. and D.T. Milne, "Drop Tests of Cones to Investigate the Three-Dimensional Effects of Slamming," NSRDC Report 3543 (Apr 1971).
8. Carnahan, B. et al., "Applied Numerical Methods," Chapter 1, John Wiley & Son, Inc., New York (1969).
9. Dinsbacher, A.L. et al., "Model Test Determination of Sea Loads on Catamaran Cross Structure," NSRDC Report 2378 (May 1967).
10. Lankford, B.W., Jr., "The Structural Design of the ASR Catamaran Cross Structure," Naval Engineers Journal, Vol 79, No. 4 (Aug 1967).
11. Lee, C.M., et al., "Prediction of Motion and Hydrodynamic Loads of Catamarans," Marine Technology, Vol. 10, No. 4 (Oct 1973).
12. Hadler, J.B. et al., "Ocean Catamaran Seakeeping Design, Based on the Experience USNS HAYES," Transactions SNAME, Vol 82 (1974).
13. Ochi, M.D. and J. Bonilla-Norat, "Pressure-Velocity Relationship in Impact of a Ship Model Dropped onto the Water Surface and in Slamming in Waves," NSRDC Report 3153 (Jun 1970).